

Seismicity in a model governed by competing frictional weakening and healing mechanisms

G. Hillers,^{1,*} J. M. Carlson² and R. J. Archuleta^{1,3}

¹*Institute for Crustal Studies, University of California, Santa Barbara, CA 93106, USA. E-mail: gregor@gps.caltech.edu*

²*Department of Physics, University of California, Santa Barbara, CA 93106, USA*

³*Department of Earth Science, University of California, Santa Barbara, CA 93106, USA*

Accepted 2009 April 17. Received 2009 April 16; in original form 2008 July 29

SUMMARY

Observations from laboratory, field and numerical work spanning a wide range of space and time scales suggest a strain dependent progressive evolution of material properties that control the stability of earthquake faults. The associated weakening mechanisms are counterbalanced by a variety of restrengthening mechanisms. The efficiency of the healing processes depends on local material properties and on rheologic, temperature, and hydraulic conditions. We investigate the relative effects of these competing non-linear feedbacks on seismogenesis in the context of evolving frictional properties, using a mechanical earthquake model that is governed by slip weakening friction. Weakening and strengthening mechanisms are parametrized by the evolution of the frictional control variable—the slip weakening rate R —using empirical relationships obtained from laboratory experiments. In our model, weakening depends on the slip of an earthquake and tends to increase R , following the behaviour of real and simulated frictional interfaces. Healing causes R to decrease and depends on the time passed since the last slip. Results from models with these competing feedbacks are compared with simulations using non-evolving friction. Compared to fixed R conditions, evolving properties result in a significantly increased variability in the system dynamics. We find that for a given set of weakening parameters the resulting seismicity patterns are sensitive to details of the restrengthening process, such as the healing rate b and a lower cutoff time, t_c , up to which no significant change in the friction parameter is observed. For relatively large and small cutoff times, the statistics are typical of fixed large and small R values, respectively. However, a wide range of intermediate values leads to significant fluctuations in the internal energy levels. The frequency-size statistics of earthquake occurrence show corresponding non-stationary characteristics on time scales over which negligible fluctuations are observed in the fixed- R case. The progressive evolution implies that—except for extreme weakening and healing rates—faults and fault networks possibly are not well characterized by steady states on typical catalogue time scales, thus highlighting the essential role of memory and history dependence in seismogenesis. The results suggest that an extrapolation to future seismicity occurrence based on temporally limited data may be misleading due to variability in seismicity patterns associated with competing mechanisms that affect fault stability.

Key words: Seismic cycle; Earthquake dynamics; Rheology and friction of fault zones.

1 INTRODUCTION

Faults evolve, organize and interact in a fault network to accommodate relative plate motion. During this complex strain organizing process (Wesnousky 1988, 1999) the micro- and macromechanical

properties of the involved materials constantly change, as crustal rocks are continuously deformed, transported and altered as they are exposed to cyclic stresses and stress fluctuations associated with the earthquake cycle and remote earthquakes. Consequently, fault friction co-evolves in response to abrasive mechanisms, wear, progressive structural regularization and chemically driven, fluid assisted healing and restrengthening.

A number of laboratory and numerical experiments designed to isolate frictional rock properties suggest a transition from

*Now at: the Seismological Laboratory, California Institute of Technology, Pasadena, CA 91125, USA.

overall strengthening to weakening with continued deformation. In principle, an ensemble of relatively young, spatially distributed faults with rough sliding interfaces filled with unconsolidated gouge coalesces into simpler structures with ground interfaces hosting consolidated abrasive material. Friction associated with irregular sliding surfaces during initial breakup exhibits strengthening which is characterized by a relatively large fracture energy, G , required to create new fracture surface or to break prominent surface irregularities. In the seismogenic part of the crust, frictional strengthening may be a result of dilatancy or local entropic effects (effective temperature) of granular aggregates, and is thus a typical response of less consolidated wear products (Marone 1998; Langer 2008, and references therein).

Tectonically driven rock grinding processes, that is, abrasion of contact asperities and continuous grain comminution, lead to the gradual development of fault zone gouge layers (Chester & Chester 1998; Chester *et al.* 2004). The properties of gouge layers govern the evolution of the frictional resistance during dynamic instabilities and therefore the behaviour of earthquake faults (e.g. Scholz 1990; Chambon *et al.* 2006; Daub & Carlson 2008). The response of structurally simpler, relatively smooth faults with consolidated wear products is typically characterized by slip or velocity weakening, associated with smaller G values. Under these conditions, the frictional resistance drops to relatively low dynamic sliding levels, thus promoting the occurrence and propagation of large earthquakes.

The evolution of frictional properties reflects the organization of crustal and fault zone material (Ben-Zion & Sammis 2003). Dynamic friction is therefore sensitive to variable external and internal conditions, such as mechanical properties of the adjacent crustal material and gouge characteristics. Since macroscopic properties of

fault networks, but also microscopic properties of individual faults, are constantly evolving, they probably do not reach a steady state (see the Appendix for more details). A fault system may thus not equilibrate on time scales of few earthquake cycles, a consequence of the superposition of competing processes that influence the properties and stability of earthquake faults. This suggests that from one earthquake to the next, friction may not be well described by a fixed function, even in a given location on a given fault.

Acknowledging the poor constraints on *in situ* weakening and healing rates, we explore the effects of strength degradation and recovery in the context of evolving frictional properties, using a linear slip weakening friction law (Ida 1972). The friction law is defined by the material strength F_0 , the weakening rate R and the residual sliding level f_s (Fig. 1a). Conceptually, the level of f_s relative to the stress or force outside the hypocentral area at the onset of an instability influences the dynamic response and thus the slip pattern of an earthquake. Because R controls the slip $\Delta u = d_c$ necessary to reach f_s , it governs the overall friction behaviour and seismic response. We incorporate history dependence through variation of the weakening rate R with slip and time and contrast it with the fixed- R case.

Although time and history dependence is an important aspect of the rate-and-state laws, the framework does not account for the evolution of friction over long time scales and the corresponding evolution of parameters that control stability, for example, the frictional slip rate dependence (Ruina 1983). Using the rate-and-state framework in multicycle simulations, the healing controls the repetitive restrengthening after model earthquakes, but healing does not affect the dynamic regime, which does not change for a given set of parameters and boundary conditions. For rate-and-state, it is also less clear how to construct a comparison study with a scenario of

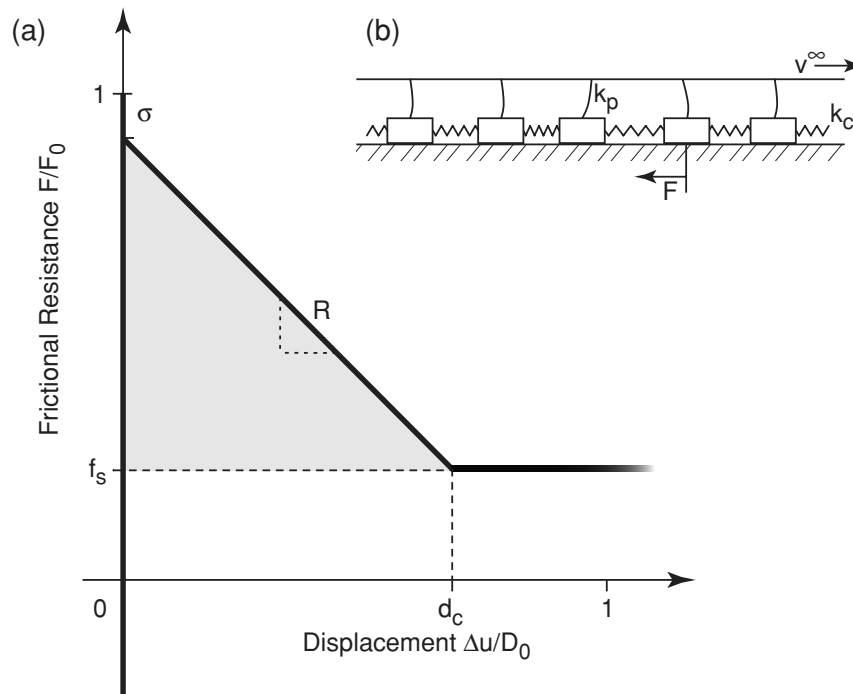


Figure 1. (a) Sketch of the slip weakening friction given in eq. (7) and (b) the mechanical model described by eq. (3). The velocity of the loader plate is v^∞ , and the loader spring and block connecting spring constants are k_p and k_c , respectively. The motion of a block is controlled by the friction in (a). If the force on a block, K , reaches the peak strength $F = F_0$, F drops to $F = F_0(1 - \sigma)$. During unstable slip $\Delta u > 0$, the frictional strength decreases with rate R to the sliding level, $F = F_0 f_s$, at $\Delta u = d_c$. The grey shaded area is proportional to the fracture energy G . The smaller G , the weaker a fault behaves, and instabilities tend to grow more easily.

evolving properties such as the slip rate dependence or the critical slip distance.

To explore long term effects of friction evolution efficiently we choose a 1-D mechanical model, that is, a Burridge-Knopoff representation of an earthquake fault as shown in Fig. 1(b) (Burridge & Knopoff 1967; Carlson & Langer 1989a). The model is governed by the slip weakening law shown in Fig. 1(a) and formally introduced in Section 3 (eq. 7). Evolution of the weakening rate R parametrizes changes in dynamic friction. Together, the primitive representation of a lateral fault and the linear slip weakening friction represent the most abstract level to investigate long term consequences of evolving friction parameters.

We focus on heterogeneity associated with dynamics as opposed to intrinsic material heterogeneity. The resulting lateral heterogeneity in R is therefore history dependent, in contrast to tuned, fixed distributions used in previous studies. Increasing and decreasing values of R correspond to transitions from relatively strong to weak conditions and vice versa. The dependence of R on slip and interevent hold time follows empirical relationships that describe phenomena observed at different spatiotemporal scales (Section 2). While previous numerical experiments mostly explored time independent friction parameters, we investigate consequences of feedbacks, friction evolution and resulting seismicity patterns. Throughout this study, the term ‘feedback’ is associated with slip and time dependent changes of the control variable R , as opposed to elastic force interactions or the ‘positive feedback’ that drives accelerating failure processes (Sammis & Sornette 2002).

Section 2 presents observations related to strength degradation and healing, and describes how the observations are parametrized in our friction model. Section 3 introduces the numerical implementation and in Section 4 we compare the results for systems with fixed versus evolving friction. We conclude with a discussion of the implications of our results for observed seismicity. The Appendix discusses in more detail additional phenomena affecting the mechanical properties of rocks and the friction behaviour of a fault and thus its seismicity.

2 WEAKENING AND STRENGTHENING PROCESSES

2.1 Weakening

The weakening of bulk properties such as the degradation of rigidity, and the change of frictional resistance governing the mechanical behaviour of sliding surfaces, depends on the deformation history. The strain dependence is deduced from observations on different scales, which suggest a progressive co-evolution of micro- and macroscopic fault characteristics. On the microscopic end, laboratory experiments that measure the decrease of the friction breakdown distance d_c (Marone & Kilgore 1993) and the increase of gouge volume (Wang & Scholz 1994), and numerical experiments on synthetic gouge thickness (Guo & Morgan 2007) show a qualitatively similar dependence on shear displacement. On the macroscopic end, field measurements of geometric fault trace heterogeneity indicate a progressive regularization of structural complexity as a function of cumulative fault offset (Wesnousky 1988). Together, these studies indicate an initially fast decrease of d_c for gouge filled surfaces, a high initial wear rate of rough surfaces, a fast increase of gouge thickness during early stages of deformation, and a rapid initial decrease of fault irregularities. The initial fast rates are consistently followed by a more gradual change at relatively larger displace-

ments, where details depend on external variables, for example normal stress.

Wang & Scholz (1994) expressed this collective behaviour in a relationship describing the gouge volume as a function of slip. Supported by the qualitatively similar behaviour of smoothing processes observed under various conditions, we approximate changes of the dynamic control variable R (the slip weakening rate, Fig. 1a) due to displacement using (Wang & Scholz 1994)

$$\Delta R^{(w)} = \left(\gamma_0 + A \frac{k_2}{k_1} \right) (1 - e^{-k_1 \Delta u}) + k_2 A \Delta u. \quad (1)$$

Eq. (1) describes the changes in R due to weakening as a function of slip, Δu . Here, γ_0 is the initial gouge volume, and A is a measure of the contact area. In our analysis γ_0 and A will not be used explicitly, but are used to scale the range of $\Delta R^{(w)}$ to appropriate values (Section 4.2.1). The wear coefficients $k_1 > 0$ and $k_2 \geq 0$ parametrize the efficiency of the wear process, and we will focus on the properties of the function controlled by k_1 . For $k_2 = 0$, $\Delta R^{(w)}$ is proportional to $1 - e^{-k_1 \Delta u}$, where larger k_1 leads to a greater change at smaller Δu . That is, the initial slope of the function $\Delta R^{(w)} = \Delta R^{(w)}(\Delta u)$ as well as the transition between rapid and gradual increase of $\Delta R^{(w)}$ are controlled by k_1 . For $k_2 > 0$, the sum in parenthesis scales the asymptote of the $1 - e^{-k_1 \Delta u}$ term, and the third term leads to a linear increase of $\Delta R^{(w)}$ beyond the rapid-to-gradual transitions. Note that the form of eq. (1) is compatible with the power-law approximation derived by Guo & Morgan (2007), suggesting a generic character for the evolution function.

2.2 Strengthening

Restrengthening is essential for stick slip and repetitive earthquakes on faults. This section discusses the mechanical and frictional properties that are affected by healing, how these observations are implemented in our model, and the observed variability in the parameters that describe these mechanisms.

Healing can be due to one or more mechanisms, such as contact yielding, compaction, fluid assisted changes in rheology associated with stress induced dissolution and redeposition, crack closure due to ductile creep, and chemical precipitation leading to cementation and crack sealing (Li *et al.* 2006, and references therein). These mechanisms affect mostly the strength of a frictional interface, which can be a fault that has slipped or microcracks whose density and distribution control bulk elastic properties. A general observation is that friction interfaces regain strength depending on the logarithm of contact or hold time, t_h (Dieterich & Kilgore 1994). This decreasing healing rate with time has been documented in laboratory experiments (Dieterich 1972, 1978). Observations of the recovery of seismic velocities after earthquakes, and source property changes from repeating earthquakes are compatible with this behaviour (Vidale *et al.* 1994; Marone *et al.* 1995; Hickman & Wong 2001; Hiramatsu *et al.* 2005; Li *et al.* 2006).

In contrast to the $\ln(t_h)$ dependence, studies on pressure solution (Yasuhara *et al.* 2005), normal stress changes (Richardson & Marone 1999) and cohesive strengthening (Tenthorey & Cox 2006) imply a significantly faster-than- $\ln(t_h)$ healing, demonstrating the sensitivity of restrengthening mechanisms to variable conditions of a fault. Furthermore, healing rates may differ after two seemingly similar, ‘characteristic’ events, depending on details of the preceding rupture and the associated creation of fracture and flow networks.

Different strengthening mechanisms possibly affect different properties of a friction parametrization (Tenthorey & Cox 2006).

Nakatani & Scholz (2004) found that the dynamic friction evolution distance d_c is also affected by changing conditions that cause a large variability in the cutoff time t_c . Furthermore, d_c correlates with the width of gouge zones and the roughness of sliding surfaces (Marone 1998; Ohnaka 2003). For bare surfaces, the time dependent increase of contact junctions (Dieterich & Kilgore 1994) suggests that d_c —which is interpreted to be the slip that brings a new set of joints into contact—depends indirectly on time, too. For gouge filled surfaces, Marone & Kilgore (1993) found a deformation dependent reduction of d_c due to shear localization. Healing might then work against localization (Lyakhovsky *et al.* 1997a), associated with an increase in d_c , which is equivalent to an increase in the weakening rate R assuming a constant frictional sliding level (Fig. 1a). Thus in our model strengthening is implemented applying the widely observed logarithmic dependence on hold time to R ,

$$\Delta R^{(s)} = -b \ln \left(\frac{t_h}{t_c} + 1 \right). \quad (2)$$

The $\ln(t_h)$ dependence, with t_h the time elapsed since the last slip on a fault, assumes a lower cutoff time, t_c , up to which no significant increase in state or strength is observed (Nakatani & Scholz 2006). Beyond t_c , healing shows a log-linear growth with slope b . The minus sign in eq. (2) stems from the fact that stronger conditions (larger asperity contacts) are associated with smaller weakening rates (larger d_c). The values of b and t_c control the healing behaviour, and we thus use b and t_c as tuning parameters for restrengthening processes. Nakatani & Scholz (2004) observed values for $b \approx 0.01$, in agreement with previously reported rates used in the rate-and-state theory (Dieterich 1978), while measurements of the cutoff time t_c vary over many orders of magnitude and depend strongly on temperature and hydraulic conditions.

The dry experiments conducted by Dieterich (1972) at room temperature indicate t_c is of the order of 0.1–1 s for the laboratory system. However, these conditions neglect temperature dependent and fluid assisted processes at depths associated with nucleation regimes of large earthquakes (Scholz 1990). Nakatani & Scholz (2004) performed experiments that simulate a range of hydrothermal conditions and found an inverse dependence of t_c on temperature, measuring values between $t_c = 10^3$ and 5×10^4 s. Moreover, healing on natural faults suggests t_c may be as large as 9×10^6 s (Marone *et al.* 1995). Nakatani & Scholz (2006) concluded that t_c is not an intrinsic constant of the healing process, and t_c may depend on the state immediately after a slip event.

Choosing different combinations of the weakening and healing parameters k_1 , k_2 (eq. 1), and b , t_c (eq. 2), respectively, we investigate the properties of synthetic seismicity of a mechanical earthquake fault model discussed next.

3 SIMULATION STRATEGY

3.1 Numerical implementation

We use a 1-D Burridge-Knopoff (Burridge & Knopoff 1967) model of a spring-slider chain connected to a loader plate moving with velocity v^∞ as shown in Fig. 1(b) (Carlson & Langer 1989a,b; Carlson *et al.* 1991). The individual mass of the n blocks is m , the strength of the slider connecting springs is k_c , and k_p is the strength of the leaf springs between the loading substrate and each sliding element. The term F is the slip dependent friction law discussed below. With x_i denoting the displacement of block i measured from equilibrium position, the equations of motion for this system are

(overdots represent time derivatives)

$$m\ddot{x}_i = k_c(x_{i+1} - 2x_i + x_{i-1}) - k_p v^\infty - F. \quad (3)$$

See Xia *et al.* (2005) for solution strategies. In eq. (3) the sum of the first and second term on the right-hand side at a time t is the elastic force or stress acting on an element, $K_i(t)$. The average stress or strain energy in the system, which is dominated by the average position of the blocks with respect to the position of the loader plate, is the normalized sum of $K_i(t)$ over all blocks,

$$E(t) = n^{-1} \sum_{i=1}^n K_i(t). \quad (4)$$

The corresponding standard deviation, a measure of stress or energy fluctuations associated with the variability of block spacings, is estimated using

$$\delta E(t) = \left\{ n^{-1} \sum_{i=1}^n [K_i(t) - E(t)]^2 \right\}^{1/2} \quad (5)$$

(Ben-Zion *et al.* 2003), and the temporal averages of these measurements are denoted as \bar{E} and $\delta \bar{E}$, respectively. Values of E and δE are scaled respectively by the maximum possible internal energy, E^* , and a value corresponding to large fluctuations, δE^* . Inspection of eq. (3) reveals that E^* is identified with F_0 , assuming a configuration at rest and equally spaced blocks. Recall that F_0 is the peak strength of the frictional interface. Similarly, δE^* is derived assuming a distribution of random block offsets x_i drawn from a uniform probability distribution in the interval $[0, 1]$. Such a configuration is extremely unlikely to occur during the evolution of the system, and not observed during our numerical experiments. The offsets are scaled to equilibrate the driving force and the frictional strength at the position where the k_c -term in eq. (3) is maximum. For the parameters given below $\delta E^* = 1.13$, found by averaging δE computed from 10^4 random block offset configurations.

Slip is measured in $u_i = x_i/D_0$, with $D_0 = F_0/k_p$, the maximum distance the loader plate can move before a block starts slipping. The characteristic loading time is $t^* = D_0/v^\infty$, that is, the time required for the loader plate to move the maximum displacement before a block starts slipping. Constant parameters used throughout this study are $n = 5000$, $m = 1$, $k_p = 40$, $k_c = k_p l^2$, $l = 10$, $F_0 = 3$, $v^\infty = 10^{-9}$, and the dynamic time step during integration using a fourth order RK method (Press *et al.* 1992) is $\delta t = 0.001$. The size of an event is measured in the equivalent of seismic potency, the integral slip over the slipped area, which reduces to

$$P = \sum_{j \in I} \Delta u_j, \quad (6)$$

where I denotes the subset of blocks that slipped during an event. Consequently, P is measured in units of slip.

Previous studies focused on the model behaviour as a function of the friction term F in eq. (3), and used different versions of a velocity weakening friction law. Here we use slip weakening friction of the form

$$F = \begin{cases} F_0 (\max[f_s, 1 - \sigma - R \Delta u]), & \text{if } \Delta u > 0 \text{ (block is slipping);} \\ (-\infty, F_0], & \text{if } \Delta u = 0 \text{ (block is at rest).} \end{cases} \quad (7)$$

Here, f_s is the frictional sliding level, $\sigma = 0.01$ approximates an infinitesimal drop in frictional resistance once the threshold F_0 is exceeded (Carlson *et al.* 1994), and R denotes the weakening rate, given in units of F_0 and D_0 . That is, for $R = 1$, $\sigma = 0$ and $f_s = 0$

friction drops from $F = F_0$ to $F = 0$ over the distance $\Delta u = D_0$ (Fig. 1a).

In Section 4, we perform simulations using fixed, time independent R values, and later sections discuss slip and time dependent changes of the slip weakening rate. To apply the feedback rules in eqs (1) and (2), the weakening rate is adjusted as follows. Let t_1 and t_2 denote the times of two successive instabilities at position i . Then R_i^{1-} and R_i^{1+} denote R_i immediately before and after the instability at t_1 , and R_i^{2-} is the value at the onset of slip at t_2 . As discussed in Section 2.1, slip weakens an interface, and this weakening is parametrized by a slip dependent increase in R_i

$$R_i^{1+} = \min \left[R^{(u)}, R_i^{1-} + \Delta R_i^{(w)} \right], \quad (8)$$

where $\Delta R^{(w)}$ is sensitive to choices of k_1 , k_2 (eq. 1). That is, the amount $\Delta R^{(w)}$ is added to the value at the onset of the instability, R_i^{1-} , but the new value R_i^{1+} does not exceed the upper bound $R^{(u)}$. Note that the value of R_i is adjusted after the event, but the friction behaviour of a block is governed by R_i^{1-} , and does not change during the event. At t_2 , the onset of the next instability at position i , the time $t_h = t_2 - t_1$ is determined and R_i adjusted according to

$$R_i^{2-} = \max \left[R^{(l)}, R_i^{1+} + \Delta R_i^{(s)} \right], \quad (9)$$

where $\Delta R^{(s)}$ depends on b and t_c (eq. 2). Recall that $\Delta R^{(s)}$ is negative, and the weakening rate thus decreases down to a minimum value $R^{(l)}$. The upper and lower bounds of the R range, $R^{(u)}$ and $R^{(l)}$, are discussed in Section 4.1.1 We assume a separation of time scales, that is, we assume a zero load velocity limit ($v^\infty = 0$ during instabilities) that prevents temporal overlap of consecutive but spatially separated events.

All discussed results consider data recorded after the initial transients. The system size has been taken to be sufficiently large that we avoid finite size effects. The ratio of the number of blocks involved in the largest events, n_l , to the system size, n , never exceeds $n_l/n = 0.45$, and in most cases is significantly smaller.

3.2 Dynamic control variables

Before we turn to simulation results (Section 4), we discuss the friction parameters F_0 , R and f_s . The frictional strength F_0 determines the maximum load an interface can sustain. Because of heterogeneous material properties of crustal rocks, and spatially variable restrengthening mechanisms (Section 2.2) the evolution of heterogeneous distributions of F_0 is physically plausible. For simplicity we ignore this material source of heterogeneity in our model which would require a more elaborate scheme to determine t and i for the next nucleation. It would also lead to spatiotemporal changes in the characteristic distance $D_0 = F_0/k_p$, which would make it more difficult to identify the involved length and time scales appropriately. For reasons of computational simplicity we therefore refrain from changing F_0 as a function of slip or time and set $F_0 = \text{const.}$, and vary R and f_s .

In Section 4.1, we consider the behaviour of the system in response to a range of fixed friction parameters R and f_s . First, we assume a constant frictional sliding level f_s . A large (small) weakening rate, R , corresponds to a small (large) fracture energy, G (Fig. 1a). Relatively large (small) values of R do (do not) allow F to drop to $F_0 f_s$ over the distance $\Delta u = d_c$, leading to effective weakening (strengthening). Recall that strengthening and weakening are associated with the dynamic response of unconsolidated, disorganized granular aggregates and solidified crustal material, respectively (Section 1).

Second, we test the implications of a change in the residual sliding level, f_s , which controls the strength drop when F_0 and R are both held constant. Changes in f_s reflect the observation that the degree of surface roughness correlates with the steady state friction coefficient. That is, for a fixed R strengthening occurs more rapidly for larger values of f_s , which implies a reduced possibility of rupture propagation. The potential effect of variable f_s is indicated by the 3-D studies of Zöller *et al.* (2005) and Mehta *et al.* (2006), who use the strength drop as a heterogeneity and tuning parameter, respectively.

4 RESULTS

4.1 Time invariant homogeneous frictional conditions

We find that the system dynamics are most sensitive to the weakening rate, R , and relatively insensitive to changes in the frictional sliding level, f_s . Using a constant value for f_s , $R < 1$ suppresses large instabilities; consequently, slip is accumulated by a large number of small events, which is reflected by an overall high stress or strain energy level in the system. For $R > 1$, two separate populations develop, and the system is dominated by large characteristic events of a certain preferred size. This leads to an overall lower level of energy, while stresses fluctuations are larger compared to the $R < 1$ -case due to the occurrence of large, stress releasing events.

4.1.1 Statistical properties

This section quantifies how slip patterns and the corresponding frequency-size statistics change as a function of fixed homogeneous friction parameters R and f_s . Fig. 2 shows slip evolution patterns in response to a constant frictional sliding level, $f_s = 0.5$, and variable weakening rates, R . The relatively large fracture energy G associated with a small weakening rate results in frictional strengthening, prohibiting accelerated, unstable slip (Fig. 2a). This is also reflected in significantly reduced slip rates during ruptures compared to instabilities governed by larger R values, and the events in Fig. 2(a) have thus a creep-like character. Larger rates R lead to conditions that favour unstable slip (Figs 2b and c), because there is less dissipation. For intermediate values ($R = 1$), the system exhibits a broad range of event sizes, compared to large values ($R = 2$) for which the energy release is dominated by the occurrence of very large events.

The largest events for $R = 0.5$ involve approximately as many blocks as the large events for $R = 2$, and hence show the same delocalized character, but have two orders of magnitude less slip. The small offsets imply a relatively regular block spacing, leading to approximately equally strained loader springs, and the forces K_i are close to the failure strength F_0 . This synchronization is a result of low offsets during an unstable slip event, and is also reflected by the high internal energy level, E , discussed below. In the three cases shown in Fig. 2, small events are confined to localized regions.

The system produces a wide range of event sizes, with the potency P spanning five orders of magnitude for $R = 0.5$, and the range increases for $R > 0.5$. Figs 3(a)–(d) show frequency-size statistics produced by systems with $f_s = 0.5$ and $R = [0.5, 1, 1.3, 2]$ (cf. Fig. 2). For values smaller than $R \approx 1$ friction does not drop to low residual levels during unstable slip, which suppresses the propagation of instabilities and the accumulation of coseismic slip. The corresponding seismicity distribution exhibits Gutenberg–Richter (GR) power-law scaling for small, localized events. The distribution is truncated by an exponential tail, indicating the lack of very large events (Figs 2a and b, 3a and b). In the earth, this feature is

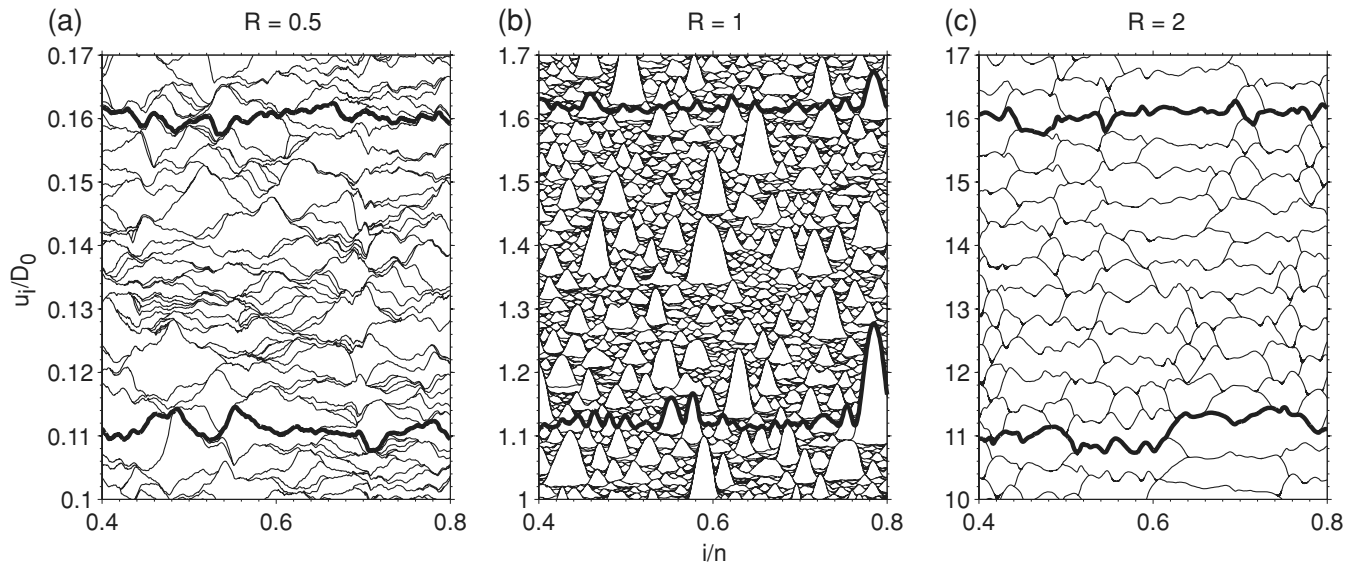


Figure 2. Spatiotemporal slip patterns for systems with $f_s = 0.5$ and variable values of the slip weakening rate, R . The horizontal lines represent the position of blocks after each slip event. In (a)–(c) thick solid lines are drawn every $0.05t^*$, $0.5t^*$ and $5t^*$, respectively. The abscissa denotes the position of individual blocks, i , as a fraction of the system size, n . Note the magnitude differences on the ordinate, necessary to visually capture the system characteristics. (a) A small weakening rate, associated with a large fracture energy, prohibits the accumulation of slip during instabilities and reflects overall strengthening. (b) $R = 1$ leads to increased slip during unstable episodes and consequently the slip pattern consists of larger events. (c) Large, delocalized events dominate the system response due to a relatively large weakening rate.

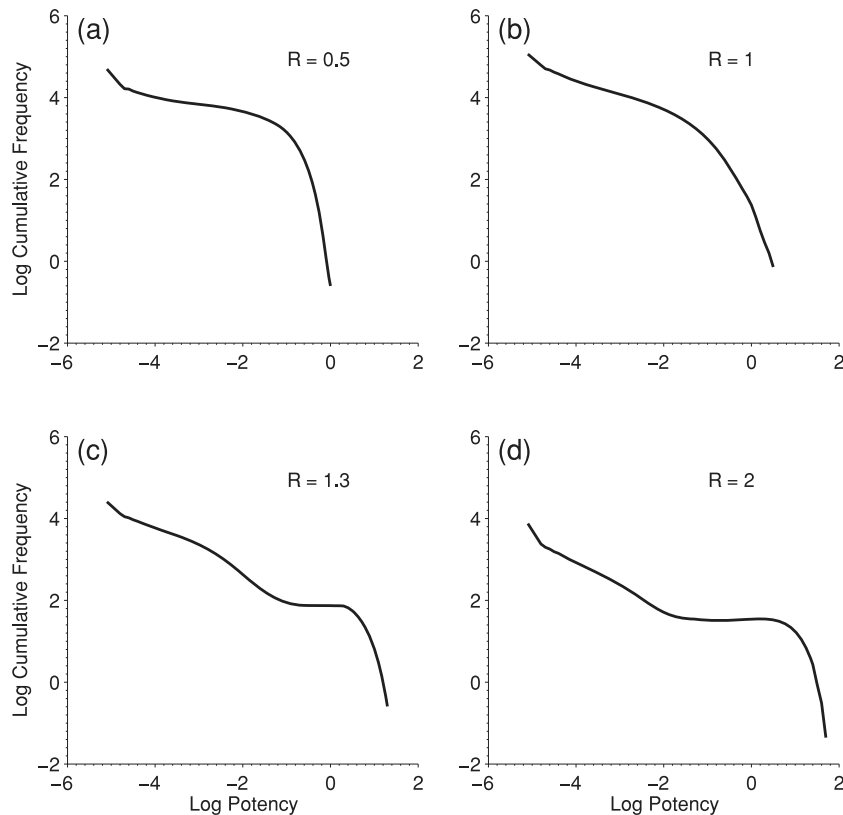


Figure 3. Frequency-size statistics of synthetic earthquakes produced by increasing weakening rates, R , and a constant frictional sliding level, f_s (cf. Fig. 2). The potency is defined in eq. (6). The frequency of occurrence is scaled to the rate per loading cycle, t^* . Relatively small R values result in an approximate power-law scaling for small and moderate events, and an exponential taper towards larger events (a and b). Larger weakening rates produce distributions that are dominated by large sizes, with an increasing gap in medium size seismicity for increasing R . The transition between these commonly referred to Gutenberg–Richter (GR) and characteristic earthquake (CE) statistics occurs around $R = 1$. The tendency to produce delocalized events associated with larger rates leads to successively larger maximum event sizes, a lower productivity (number of events per unit time), and an increase in the slope of the approximately power-law scaling small event population.

typically associated with structurally heterogeneous, immature stages of faulting (Wesnousky 1994; Stirling *et al.* 1996). As R increases in our simulations towards $R = 1$, the range of power-law scaling also increases. For $R > 1$ a separate population of very large events develops (Figs 3c and d), leading to ‘hybrid’ statistics with energy release dominated by events of a characteristic size, reminiscent of natural seismicity of structurally simpler faults (e.g. Wesnousky 1988; Ben-Zion 1996; Hillers *et al.* 2007).

The transition from the power-law scaling with exponential cutoff to a characteristic earthquake (CE) distribution with excess large events is accompanied by (1) a reduction of the overall productivity (the ‘ a ’ value in the GR scaling $\log N = a - b \log P$, with N the number of events of size P , and b the slope on a log–log plot), (2) an increased maximum event size, P^* and (3) the widening of the gap between relatively small and (very) large event populations. The opposite trend of an increase in the productivity for $R = 1$ (Fig. 3b) compared to $R < 1$ (Fig. 3a) is explained by the occurrence of local stress concentrations in the vicinity of large, approximately Gaussian shaped slip events (Fig. 2b). In general, the results are consistent with statistical properties of seismicity produced by faults at different evolutionary stages, suggested by observational and numerical evidence (Wesnousky 1988; Ben-Zion 2008).

Comparing the properties of synthetic seismicity obtained with the slip weakening law (eq. 7) to the corresponding results using velocity weakening friction verifies the importance of the weakening rate for the system dynamics (for velocity weakening friction the weakening rate α in Carlson & Langer 1989b; Carlson *et al.* 1991, 1994, plays a role similar to the slip weakening rate R in this paper). The R dependence of the event size \tilde{P} , which marks the approximate transition between small and large events, is compatible with the analysis in the Carlson *et al.* papers, where it was shown that the corresponding \tilde{P} is a function of the weakening rate parameter α . Similarly, the saturation of P^* —it does not increase for $R > 2$ —has been found to be independent of the friction response, controlled instead by the elastic properties of the system (k_c, k_p, F_0).

Fig. 4 illustrates the resulting frequency-size distributions as a function of the slip weakening rate, R , and the frictional sliding level, f_s , for a range of fixed values. The figure illustrates that the statistics are most sensitive to the weakening rate R . In this model, the strength drop, $1 - f_s$, plays only a secondary role. The relative insensitivity to the range of f_s values considered here for $R < 1$ is explained by the small offsets Δu during ‘slow slip’ events, because the relatively small R values prevent the frictional resistance F from reaching the residual level f_s . From this point on we use R as the variable friction parameter in the limits $R^{(l)} = 0.5 \leq R \leq R^{(u)} = 2$ (eqs 8 and 9), and keep $f_s = 0.5$ constant.

4.1.2 Energy measurements

Energy measurements allow us to track the temporal evolution of the system dynamics. Fig. 5 illustrates $E(t)$ and $\delta E(t)$ (eqs 4 and 5) in two systems with small ($R = 0.5$) and large ($R = 2$) weakening rates, respectively. In addition to the original data plotted after each individual slip event (black), two temporally smoothed functions of $E(t)$ and $\delta E(t)$, $E_{dt}(t)$ and $\delta E_{dt}(t)$, are shown. They are average values of E and δE from consecutive time windows of length dt and overlap $dt/2$. The figure shows two cases: for $dt = t^*/2$ (red) and $dt = t^*/10$ (blue). Trivially, a smaller time window leads to functions that are similar to the originals, whereas functions averaged over larger windows approximate the long term averages, \bar{E} and $\bar{\delta E}$.

The scaled strain energy level $\bar{E} = 0.989$ is close to unity for $R = 0.5$ (Fig. 5a) which indicates that the system is always strained to a

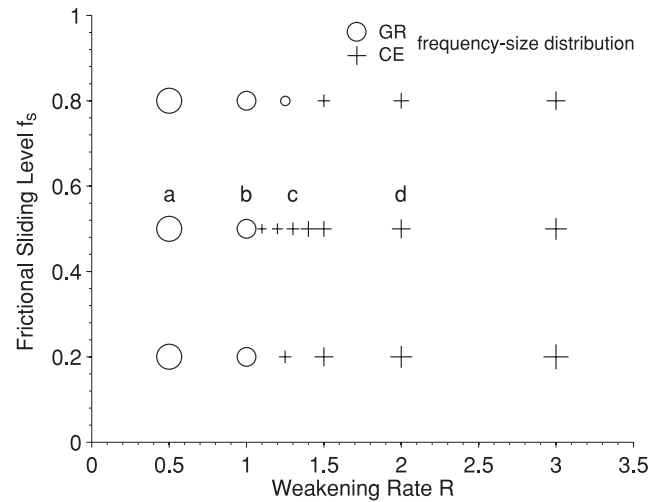


Figure 4. Overview of the observed response types as a function of the fixed dynamic variables sliding level and weakening rate, f_s and R , respectively. Circles and plus signs represent GR and CE statistics, respectively, and the symbol size represents the qualitative ‘match’ to these labels. Large circles denote approximate power-law scaling for small and moderate events and an exponential taper for larger events (Fig. 3a). Statistics associated with smaller circles show a steeper slope and a less pronounced exponential tail. Large plus signs stand for distributions that are dominated by very large event sizes, with a significant gap in medium size seismicity. For smaller plus signs the gap and the maximum event size becomes smaller (Fig. 3d). Labels ‘a’ to ‘d’ correspond to Figs 3(a)–(d). The strongest sensitivity in the system behaviour is associated with changes in R . For $R < 1$, the maximum $f_s = 0.8$ considered here is not reached during unstable slip of an individual block, which explains the constant circle size for $R \leq 1$.

very high degree, because of the inefficient weakening mechanisms associated with a small R . Conversely, the lower internal energy level in response to $R = 2$ ($\bar{E} = 0.65$) reflects the quasi-periodic occurrence of efficient energy releasing, large, delocalized events. The corresponding level of the energy fluctuations $\delta \bar{E} = 8 \times 10^{-3}$ (Fig. 5b) for low values of R are small, indicating a relatively homogeneous and synchronized system dynamics. The large amplitudes produced by the large- R model reflect significant energy changes caused by intermittent large slip events. Values around $\delta E = 0.45$ reflect a substantial degree of internal organization, compared to $\delta E = 1$ associated with random test configurations (Section 3.1).

Higher energies and smaller fluctuations are associated with stronger material properties, which prohibit the propagation of large cascading events. Correspondingly, the temporal averages \bar{E} and $\bar{\delta E}$ indicate that smaller energy levels and larger fluctuations are associated with the quasi-cyclic occurrence of delocalized events. A progression from higher to lower average values of \bar{E} and corresponding increases in $\delta \bar{E}$ is consistent with organization of fault zone material and corresponding friction evolution. As a result, fault systems progressively increase the capability for an efficient strain energy release as we demonstrate in the next section.

Fig. 6 summarizes the results of the time invariant, fixed conditions, in a E_{dt} versus δE_{dt} plane, showing results for $dt = t^*/10$ (polygons) and $dt = t^*/2$ (coloured circles). Smaller (larger) averaging time windows dt result in an increase (decrease) of the variability around the long term average, \bar{E} , $\bar{\delta E}$ (black circles). Conceptually, counter-clockwise pathways from the lower right to the upper left reflect organization and regularization of a system, associated with improved efficiency in releasing accumulated

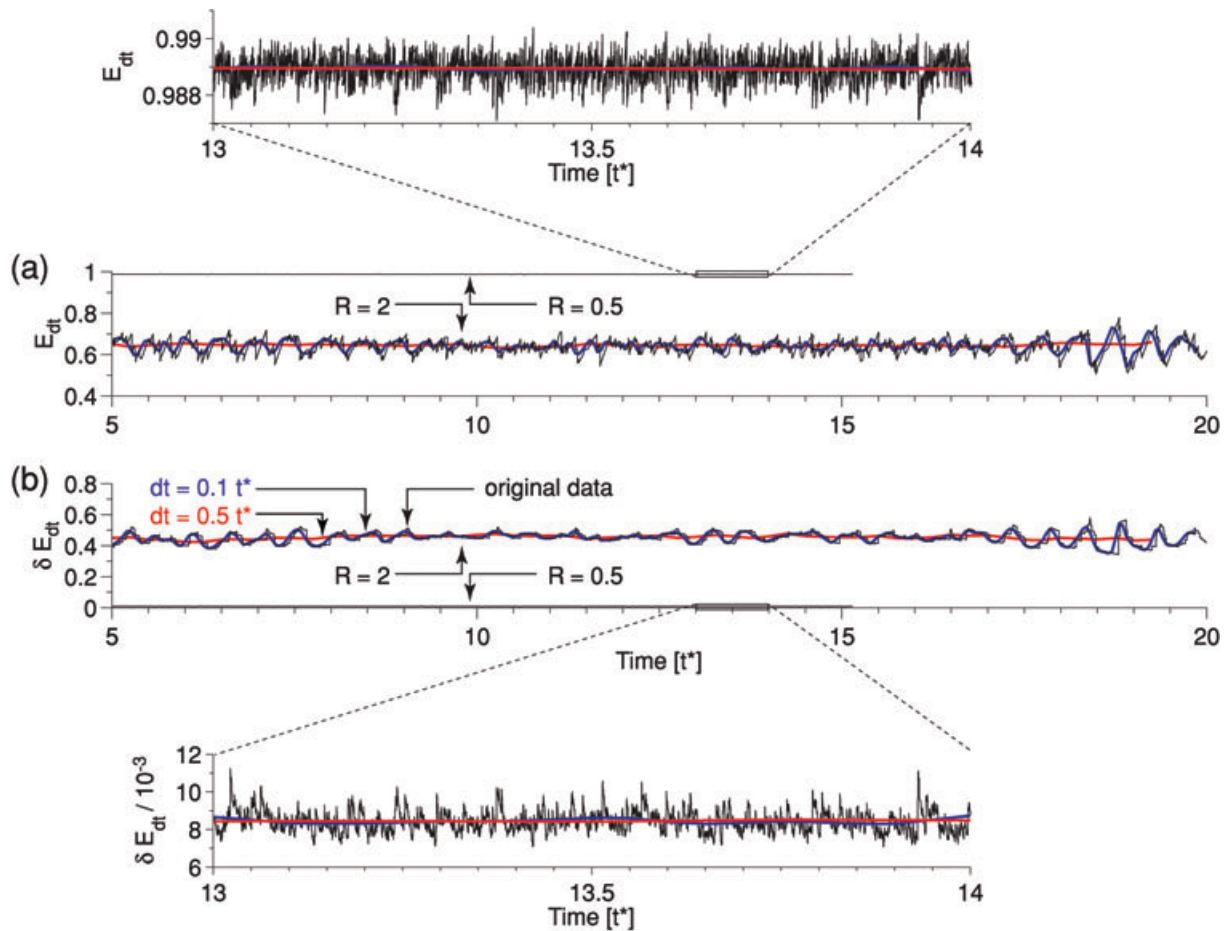


Figure 5. Temporal evolution of the (scaled) average energy (after every single event) and energy fluctuations, (a) E_{dt} (eq. 4) and (b) δE_{dt} (eq. 5), respectively, for systems with $R = 0.5$ and $R = 2$ in Figs 3(a) and (d) and 4(a) and (c). The black lines show data after each event, while the blue and red lines show values averaged over time windows of length $dt = 0.1 t^*$ and $0.5 t^*$ and overlap $dt/2$, respectively. In the small- R case the energy level close to unity implies a relatively small release of stored energy (Fig. 2a), and tiny fluctuations indicate a high degree of synchronization. Note that the functions for $R = 0.5$ in (a) and (b) appear as a straight line, and that the red line is plotted on top of the blue line in the magnified sections. The large- R system exhibits larger E_{dt} amplitudes around a lower mean level, associated with the efficient energy release of large events. Consequently, the resulting block configurations are less synchronized and exhibit higher energy fluctuations δE_{dt} .

strain energy through the production of large slip events. Opposite pathways in the E_{dt} versus δE_{dt} plane are associated with higher strength and dissipation, and coincide with an increased occurrence of small events and a reduced probability of large events. We note that we do not observe consistently directed trajectories within data sets corresponding to particular choices of R and dt , which could indicate a coherent change or evolution of system dynamics. Rather, the patterns are consistent with undirected fluctuations around the mean.

4.2 Evolving frictional properties

In summary, we find that fast (slow) healing, parametrized by relatively large (small) healing rates and small (large) cutoff times, suppress (support) the development of persistent weakening properties. For a broad range of intermediate parameter values, we observe significant fluctuations in the energy measurements on time scales that are large compared to the time scales of fluctuations in response to non-evolving friction properties. Measurements of the energy level E show that a system can intermittently be in an overall weak state (small $E \leftrightarrow$ large R), whereas at later times the properties

may exhibit strengthening characteristics. Details such as the time associated with these transitions depend on the values for b and t_c , but the qualitative results are robust over a range of parameters that control the evolution of R . This suggests that fluctuations on time scales of multiple earthquake cycles may be a generic feature of an evolving threshold system with competing frictional weakening and strengthening. The results imply that extrapolations based on past seismicity patterns possibly under- or overestimate seismicity rates at later times, depending on the potency range.

4.2.1 Feedback parametrization—length scales

To implement the weakening and strengthening processes discussed in Section 2, it is useful to consider the relevant length and time scales. We begin this discussion by revisiting the observed weakening length scales introduced in Section 2.1. From this we infer a distance d_i that characterizes the transition from initial frictional strengthening to later weakening behaviour.

In the laboratory experiments by Marone & Kilgore (1993), the initially large characteristic slip distance d_c reaches a lower, constant value for a shear strain of about 10, but the ratio between

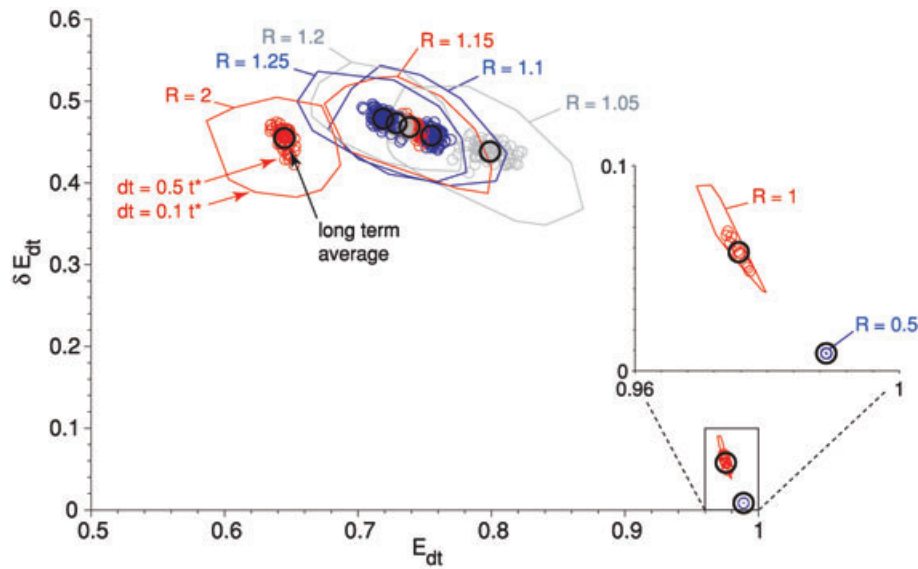


Figure 6. Representation of system dynamics in the E_{dt} (mean energy) versus δE_{dt} (energy fluctuations) plane. Data are averaged over two different time windows of length $dt = 0.1t^*$ and $0.5t^*$. The coloured circles correspond to results for $dt = 0.5t^*$, using different values of R . The polygons indicate the envelope of data points for $dt = 0.1t^*$. Similar to Fig. 5, a successive increase of dt reduces the scatter and tends to confine the data around the long term temporal average (black circles).

the initial and a later constant value depends on the gouge particle size distribution and layer thickness. In the Wang & Scholz (1994) rotary shear experiments, the change in wear rate from initially high values to reduced normal stress dependent steady state values occurs at about 10 cm. The numerical experiments by Guo & Morgan (2007) of strained particle ensembles indicate a change in plastic deformation from distributed to localized shear at a displacement of 10 mm. Note that these experiments do not simulate stick slip episodes, but continuous deformation. According to Marone (1998), the microscopic distance d_i reflects the length scale of the stability transition associated with the discussed measurements at the microscopic scale (d_c , wear rate, and localization). Since laboratory measurements need to be scaled when applied to macroscopic scales, he argues that an upscaled value of d_i might be applied to the transition from fast to gradual change of geometric fault zone heterogeneity with increasing cumulative fault offsets (Wesnousky 1988).

Therefore, we rescale the transition distance d_i associated with the discussed microscopic observations to approximate mechanisms at a larger scale. This is based on the conclusion that the breakdown distance d_c also depends on the observation scale, that is, laboratory and field estimates of d_c differ by orders of magnitude (Perfettini *et al.* 2003). Given the uncertainties in the observations related to the stability transition, we make an estimate of the transition distance d_i using a scaling factor similar to the ratio of estimates of the micro- to macroscopic characteristic slip distance (Bizzarri & Cocco 2003). Hence, the transition distance d_i in our model is equivalent to an offset $\Delta u = D_0$, assuming D_0 to be of the order of 1–10 m (Table 1).

Using eq. (1), this translates into a transformation of R from strong ($R = 0.5$) to weak ($R = 2$) conditions, restricting $\Delta R^{(w)}$ to lie between 0 and 1.5. Figs 7(a) and (b) display $\Delta R^{(w)}$, that is, the increase of R as a function of slip for different sets of k_1 and k_2 . Starting with an initial value of $R = 0.5$, different functions cross the boundary between weak and strong behaviour associated with $R \approx 1$ (Fig. 4) and thus $\Delta R^{(w)} \approx 0.5$ at different fractions of

D_0 . Fig. 7(b) illustrates that the evolution of a system is strongly controlled by the increase of R at small displacements in the initial small- R regime.

4.2.2 Feedback parametrization—time scales

As discussed in Section 2.2, values for the healing parameter b are of the order of 0.01, and the cutoff time t_c has been observed to vary by several orders of magnitude. The timescale of seconds, associated with the duration of unstable slip episodes, is related to the slipping time of a single block in our model, $\omega_p^{-1} \propto k_p^{-1/2}$ (Carlson & Langer 1989b). Figs 7(c) and (d) show the increment $\Delta R^{(s)}$ and the evolution of R as a function of the time a block is at rest, t_h , $R(t_h) = R(t_h = 0) + \Delta R^{(s)}(t_h)$ (eq. 2), for different values of the parameters b and t_c . For values of $b = 0.01$ the time required for total healing ($\Delta R^{(s)} = -1.5$, $R = 2 \rightarrow 0.5$) barely counterbalances increases in R associated with maximum displacements of the order of D_0 , with an approximate repeat time t^* ($R > 1$). However, the magnitude of maximum slip during instabilities in the initial small- R regime is much less than D_0 , about $10^{-4}D_0 < \Delta u < 10^{-2}D_0$. According to Fig. 7(b), slip of this magnitude increases R in the range of 0–0.3, depending on k_1 and k_2 . Hence, a subsequent change of $-\Delta R^{(s)}$ of similar magnitude is necessary to reach the starting level $R = 0.5$, to keep the system in the strengthening regime.

Because the value of the macroscopic stability transition distance ($d_i = D_0$) is less well constrained by data than direct measurements of b and t_c , we focus on results using one set of parameters $k_1 = 0.4$ and $k_2 = 0$. The implications of different choices will be separately discussed. Choosing $d_i = D_0$ leads to ranges of $\Delta R^{(w)}$ in the small- R regime that can be counterbalanced by $-\Delta R^{(s)}$ using $b = 0.01$, a value typically observed in experimental situations. We will use a fixed weakening parametrization, values around $b = 0.01$, together with systematic variations of t_c (Table 1). As demonstrated in the following sections, our numerical experiments cover a large range of system behaviour without using extreme parameter choices, that

Table 1. Summary of the length and time scales associated with weakening and healing mechanisms discussed in the text.

	Observation	Scale	Context/conditions	Model implementation
Weakening	(i) Displacement at which d_c reaches a lower, constant value	10^{-3} m	Laboratory experiments of friction with gouge	Upscale observations from microscopic scales (i)–(iii) to account for macroscopic conditions; use upscaled stability transition distance $d_t = D_0$ (~ 10 m)
	(ii) Displacement at which accumulation of gouge changes	10^{-2} m	Numerical experiments of particle ensembles	
	(iii) Displacement at which wear rate changes	10^{-1} m	Laboratory experiments of frictional surfaces	
	(iv) Displacement associated with regularization of fault traces	10^5 m	Measurement of fault zone heterogeneity	
Healing	Healing rate b	10^{-2}	Measurements in friction experiments	Use $b = 0.01$ and $b = 0.02$.
	cutoff time t_c	$1-10^5$ s	Measurements in friction experiments with variable hydrothermal conditions	Use $5 \leq t_c \leq 2 \times 10^5$ s

Notes: The relevant references are given in Sections 4.2.1 and 4.2.2. The displacements in (i)–(iv) refer to a distance d_t associated with the transition from strengthening to weakening behaviour. This transition corresponds to the localization of deformation in gouge layers in (i)–(iii), and to the reduction of fault trace heterogeneity in (iv) that allows large ruptures to propagate.

Table 2. List of symbols, ordered column-wise in the order of appearance.

R	Linear slip weakening rate	k_c, k_p	Spring constants	σ	Friction drop
b	Healing rate	F	Frictional resistance	t_1, t_2	Times of instabilities
t_c	Healing cutoff time	x	Block displacement	R^{1-}, R^{1+}	R before/after instability 1
G	Fracture energy	i, j	Position index	R^{2-}	R before instability 2
F_0	Max. shear resistance	t	Time	$R^{(u)}$	Upper bound of R
f_s	Frictional sliding level	K	Elastic force	$R^{(l)}$	Lower bound of R
Δu	Slip during instability	E	Average stress	n_l	Blocks per event
d_c	Slip weakening distance	δE	Standard deviation of E	N	No. of events in GR statistics
$\Delta R^{(w)}$	Weakening change in R	$\bar{E}, \delta \bar{E}$	Temporal averages of $E, \delta E$	a, b	Productivity, slope in GR stats.
γ_0, A	Gouge volume, contact area	$E^*, \delta E^*$	Max. values of $E, \delta E$	P^*	Max. event size
k_1, k_2	Wear coefficients	u	Scaled displacement	α	Weakening rate
t_h	Hold time	D_0	Char. loading distance	\tilde{P}	Transition size
$\Delta R^{(s)}$	Strengthening change in R	t^*	Char. loading time	$E_{dt}, \delta E_{dt}$	$E, \delta E$ smoothed
v^∞	Load velocity	δt	Numerical time increment	dt	Smoothing time window
n	Number of blocks	P	Seismic potency	d_t	Transition distance
m	Mass of slider block	I	Subset of slipped blocks	ω_p	Block slipping time

illustrates the distinction between systems with fixed and evolving friction.

4.2.3 System dynamics—energy measurements

Similar to Sections 4.1.1 and 4.1.2 we use frequency-size statistics and energy measurements to analyse the dynamics of systems with evolving friction. We contrast these results to our previous results for fixed friction parameters. We begin with the discussion of energy measurements, and conclude with examples of frequency-size statistics.

We set the parameters $k_1 = 0.04$ and $k_2 = 0$ (Figs 7a and b) which leads to a relatively rapid transition from stronger to weaker material properties. Fig. 8 displays measurements of E_{dt} and δE_{dt} for $b = 0.01$, $b = 0.02$ and variable cutoff times, t_c . All simulations start with $R = 0.5$. Data are recorded beginning at time $t = t^*$ after the initial transients have passed. The competing weakening and strengthening feedbacks start operating at $t = 2t^*$. Visual inspection of energy measurements indicate that the transients associated with the beginning of the feedbacks do not last longer than approximately $3t^*$ to $5t^*$. The discussion of system dynamics in response

to evolving friction considers data unaffected by these transients ($t > 5t^*$).

In Fig. 8(a) ($b = 0.01$), a small cutoff time $t_c \leq 10$ s (grey, green data) keeps the system in the small- R regime. This is because healing starts with a very short delay and thus counterbalances slip dependent increases of R soon after an event terminates. However, compared to the ‘small- R reference’ results displayed in Fig. 5 the $t_c \leq 10$ s cases (Fig. 8) develop significant deviations of E_{dt} and δE_{dt} from the seemingly straight lines $E_{dt} = 0.989$ and $\delta E_{dt} = 8 \times 10^{-3}$. This indicates that the competition between weakening and strengthening influences the system dynamics, leading to intermittent conditions allowing large events to occur. Further reduction of the cutoff time t_c results in progressive suppression of the fluctuations. Systems with $t_c \geq 50$ s exhibit dynamics corresponding to an overall weaker regime, indicated by smaller (larger) E_{dt} (δE_{dt}) levels. Fig. 8(a) indicates that at the large end of the t_c range considered here (blue data), the healing induced increases of R are too small to effectively counterbalance weakening. Consequently, the energy measurements do not differ significantly from the fixed ‘large- R reference’ case (Fig. 5). The responses to t_c in the range 10 to 100 s (Fig. 8 red, black data) indicate that the respective systems show significantly larger fluctuations of E_{dt} on time scales of tens

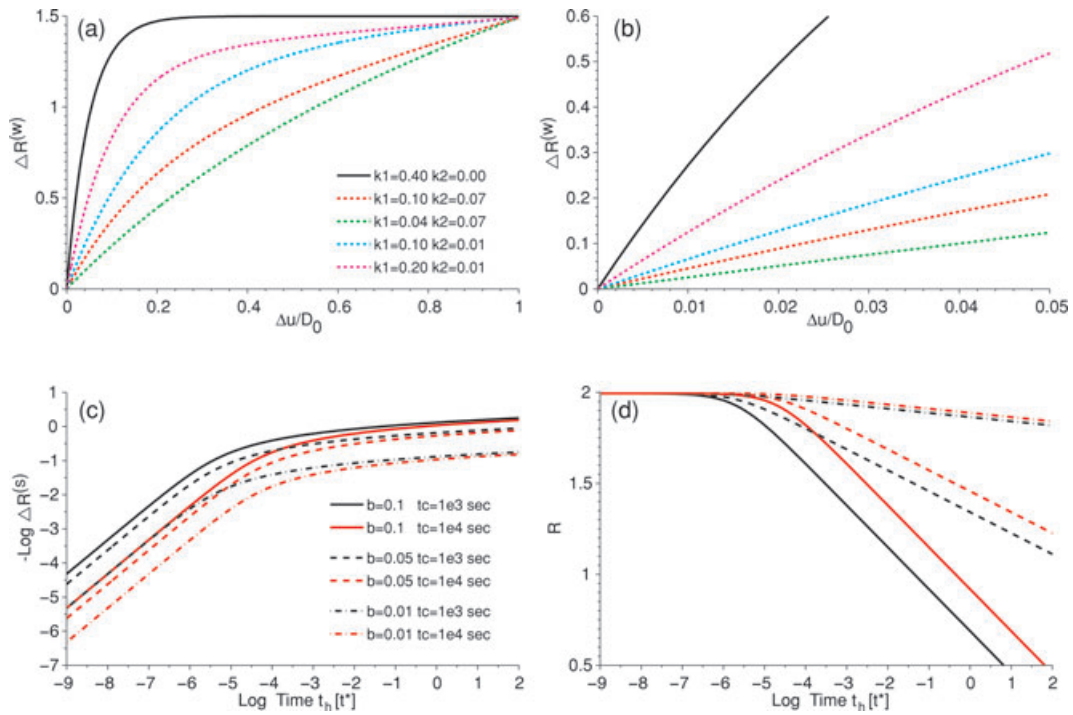


Figure 7. Graphical representation of the evolution functions representing weakening (eq. 1) and healing (eq. 2), obtained from interpretations of laboratory experiments by Wang & Scholz (1994) and Nakatani & Scholz (2004, 2006), respectively. (a) Slip induced weakening of $\Delta R^{(w)}$, depending on k_1 and k_2 . The scaling parameters of eq. (1), γ_0 and A , have been chosen appropriately to change R from 0.5 to 2 (cf. Fig. 4) over the sliding distance $\Delta u = D_0$, that is, $\Delta R_{\max}^{(w)} = 1.5$. (b) Magnification of (a) for small offsets. (c) Changes in R as a function of hold time, t_h , for different combinations of the healing parameter b , and the cutoff time, t_c . (d) Illustration of eq. (9), with $R^{1+} = 2$ and $\Delta R^{(s)}$ as in (c).

of loading cycles. Interestingly, the level of energy variations δE_{dt} are higher compared to the case $t_c = 10^3$ s (blue data), which shows a lower E_{dt} . This illustrates that conditions in which weakening and strengthening conditions are roughly balanced produce the largest variability (fluctuations in E , level of δE) in the system dynamics.

A qualitatively similar response to increasing t_c is observed using $b = 0.02$ (Fig. 8b). The increased healing rate shifts the relevant range of t_c to larger values, $t_c = 2 \times 10^3$ to 20×10^3 s, to obtain results similar to Fig. 8(a) with $b = 0.01$. For the smallest $t_c = 10^3$ s (grey data) considered here, the system dynamics are almost identical to the fixed- $R = 0.5$ case, that is, healing dominates the response. Larger t_c (green, red and black data) results in energy measurements similar to the $b = 0.01$ case, showing a progressive decrease of the energy level E , fluctuations of E over time intervals which are long compared to the fixed- R simulations, and an increase in the energy variations δE at a given time.

For the largest cutoff time, $t_c = 2 \times 10^4$ s (blue data), weakening dominates and the dynamics are similar to the fixed- $R = 2$ case.

We performed additional simulations using different weakening curves (eq. 1 with different values of k_1, k_2 ; dashed lines in Fig. 7a). For a given coseismic offset Δu , a smaller value of $\Delta R^{(w)}$ requires a smaller healing rate or larger cutoff time to evolve towards weaker large- R conditions. A reduction of d_t to values smaller than D_0 (Figs 7a and b) together with larger healing rates or smaller cutoff times has a similar effect.

Fig. 9 displays the temporal behaviour of the systems discussed in Fig. 8 in the E_{dt} versus δE_{dt} plane, showing typical evolution paths for different values of the weakening and healing rates. The trajectories depend on b and t_c , and except for limiting values the fluctuations— δE as well as the range of δE and E —are large compared to the fixed- R cases (Fig. 6). The data indicate a transition

from strengthening to weakening dynamics. Strengthening (weakening) dynamics are characterized by a high (low) energy level E , a large (small) variability of δE at a relatively low (high) δE level. The results are sensitive to the time window dt , but are found to be robust for $dt \geq 0.5t^*$ (Fig. 9c). In the examples with a relatively small cutoff time t_c , periods of reduced energy E due to the occasional occurrence of large events increase the variability, indicated by significant changes in δE . However, the reductions in E are small, because the frictional properties of only a limited set of blocks I has undergone significant change. Because of the longer periods the involved sliding elements $i \in I$ are at rest, their R values recover to the minimum value, $R^{(l)}$. A qualitatively similar behaviour is observed for larger cutoff times. Fig. 9(d) expands a section of data from $10t^*$ (Fig. 8b, black data), sampling E_{dt} and δE_{dt} values with $dt = 0.5t^*$. Progressively darker shades of grey illustrate the temporal evolution, indicating a period of significant strengthening (clockwise pathway) followed by weakening (opposite trajectory). Though this type of pattern is consistently observed in the dynamics, we do not observe a systematic temporal pattern for the time ranges considered.

4.2.4 Frequency-size statistics

While the analysis of E and δE measurements permits a detailed analysis of our numerical simulations, the corresponding observations cannot be made on real faults. To discuss properties that are observable, we consider temporally variable properties of synthetic frequency-size statistics. Fig. 10 shows three examples of frequency-size distributions from simulations with $b = 0.02$ (Fig. 8), where the corresponding subcatalogues contain seismicity for five consecutive time windows of duration $2t^*$, covering data from

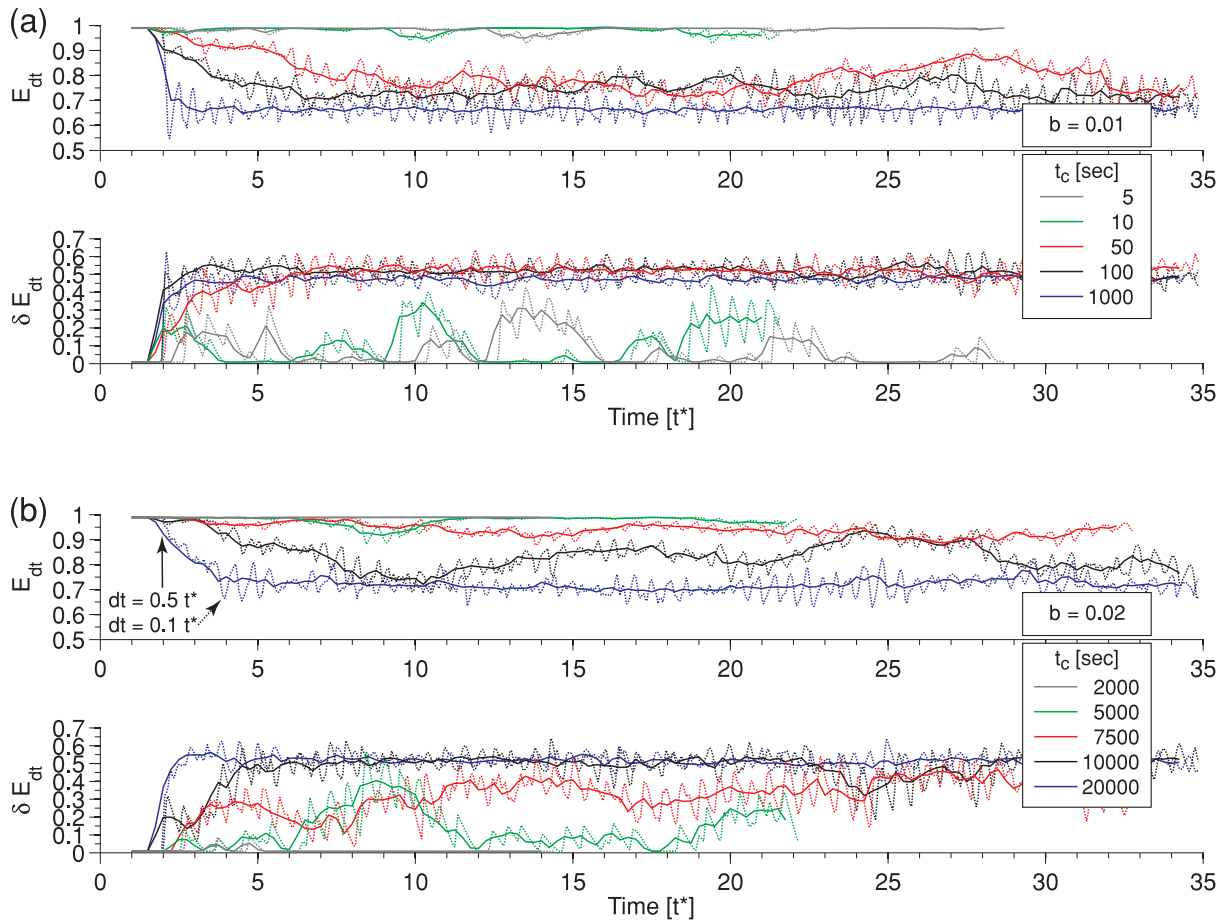


Figure 8. Temporally averaged values of E_{dt} and δE_{dt} , with $dt = 0.1 t^*$ (dashed) and $dt = 0.5 t^*$ (solid), from simulations with variable values of the healing parameter b and t_c . The weakening parameters are held constant, using the values that correspond to the black line in Figs 7(a) and (b).

$t = 5 t^*$ to $15 t^*$. Differences in seismicity rates for a given potency P in subsequent time windows vary for different values of t_c . In Fig. 10(a), occurrence rates for smaller events are relatively constant, while the frequency of occurrence for events with $P > 10$ can differ by an order of magnitude between successive sub-catalogues. The changes are significant compared to the data in the inset, showing statistics of five consecutive $2 t^*$ sub-catalogues from fixed- R cases, where no differences can be observed. Note that the results are robust with respect to the time window chosen (not shown). Models with larger values of t_c (Figs 10b and c) show less pronounced changes at larger potencies, but an increasing change in medium-size seismicity with $10^{-4} < P < 10$. Seismicity rates for large potencies show the largest variability when the dynamics alternate between weakening and strengthening behaviour (e.g. for $b = 0.02$, $t_c = 5 \times 10^3$ s). The changes in seismicity rates are less significant in situations dominated by weakening or strengthening (e.g. for $b = 0.02$, $t_c = 10^4$ s), yet indicate effects of continuous changes in the frictional properties.

5 DISCUSSION

5.1 Fault zone dynamics

We compare our results to previous models that simulate fault zone dynamics. We deliberately parametrize friction evolution in a relatively simple way, following a large body of field and laboratory

measurements that are most often parametrized using slip weakening models. Slip weakening is also widely used as a starting parametrization for earthquake simulations, and it is straightforward to construct a case with non-evolving friction. Furthermore, we find that our observations are compatible with models of higher dimensionality and larger internal degrees of freedom, which use a more detailed but computationally more expensive description of physical mechanisms associated with faulting.

Several studies using multicycle simulations explore systematically the effects of frictional and mechanical parameters that control fault zone stability, and discuss the properties of the resulting synthetic seismicity patterns (e.g. Carlson 1991; Rice 1993; Ben-Zion 1996; Langer *et al.* 1996; Fisher *et al.* 1997; Dahmen *et al.* 1998; Lapusta *et al.* 2000; Shaw & Rice 2000; Weatherley *et al.* 2002; Heimpel 2003; Zöller *et al.* 2005; Mehta *et al.* 2006; Hillers *et al.* 2007). Properties such as the energy dissipation and stress interaction distance, dimension, the degree of heterogeneity, and the range of size scales have been used as control parameters. Across a broad range of dimensionality and details of the individual parametrization, structurally disordered faults associated with highly dissipative friction are observed to produce power-law statistics compatible with the GR distribution of seismicity. Relatively homogeneous conditions in tandem with frictional weakening mechanisms lead to slip dominated by CE with a certain preferred size. These seismicity patterns have been discussed in the context of decreasing geometrical heterogeneity and increasing fault maturity of real faults (Wesnousky 1988, 1994; Stirling *et al.* 1996).

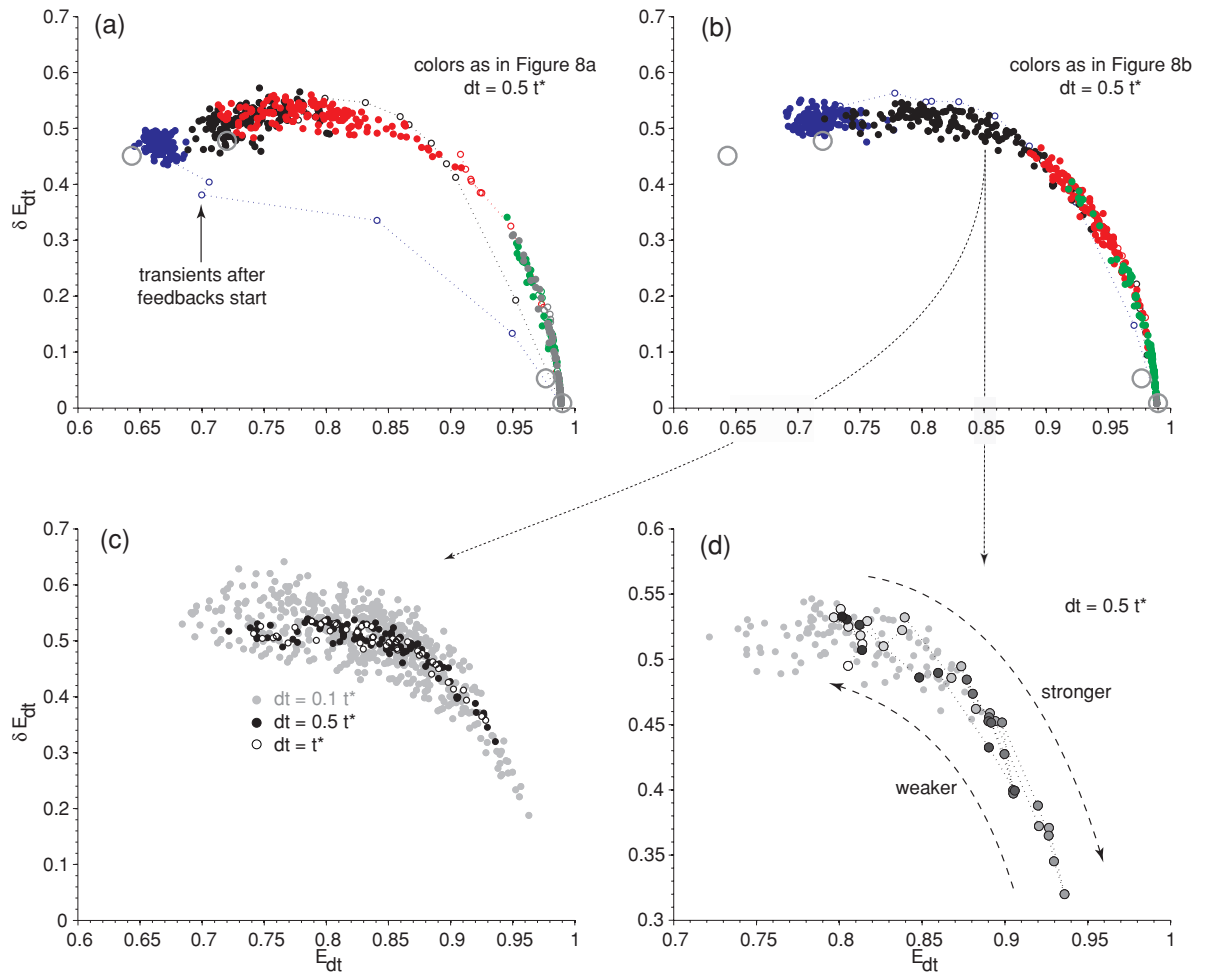


Figure 9. Representation of the data shown in Fig. 8 in the E_{dt} versus δE_{dt} plane. (a) & (b) Small open circles denote the transient effects after the feedbacks started to operate. The four grey circles correspond to the stable mean values of the systems with fixed properties discussed in Fig. 6. Here, $dt = 0.5 t^*$. (c) & (d) Data from (b), $b = 0.02$, $t_c = 10^4$ s. (c) Data averaged over three different time windows, $dt = 0.1 t^*$, $dt = 0.5 t^*$, and $dt = t^*$. (d) Light grey dots show data for all times, while progressively darker circles illustrate the temporal evolution for $20 t^* < t < 30 t^*$ (Fig. 8b, black). A $5 t^*$ -period of motion towards more strengthening behaviour is subsequently reversed.

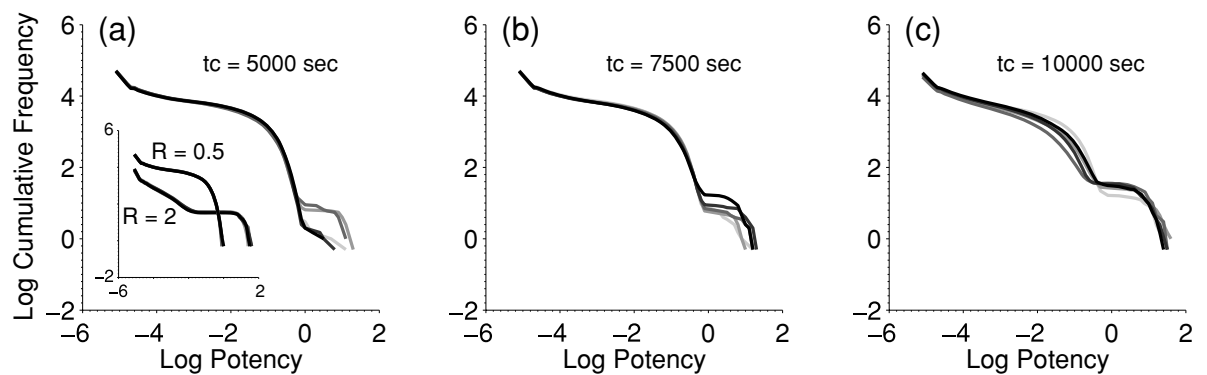


Figure 10. Evolution of temporal seismicity patterns for three systems with $b = 0.02$ discussed in Fig. 8(b). Shown are the frequency-size distributions of five consecutive subcatalogues containing seismicity from two loading cycles ($2 t^*$), covering the period between $t = 5 t^*$ and $15 t^*$. The inset in (a) displays the (non) evolution of the frequency-size distribution for models with fixed R (Fig. 3). Successively darker shades of grey indicate later time periods. The fluctuations suggest that extrapolations based on previous system dynamics possibly under- or overestimate future earthquake occurrence.

Results from our fixed- R simulations are conceptually comparable to these findings. The small- (large-) R results are qualitatively similar to results obtained in models with high (low) energy dissipation (Zöller *et al.* 2005) and small (large) dynamic weak-

ening (Carlson *et al.* 1991; Mehta *et al.* 2006). These are conceptually similar parametrizations of large (small) fracture energies, which suppress (support) tendencies for rupture propagation. These conditions are associated with structurally heterogeneous

(homogeneous) fault architectures, characterized by a large (small) range of size scales (Ben-Zion 1996, 2001; Zöller *et al.* 2004; Hillers *et al.* 2006, 2007).

However, to date most models have used time independent variations of the control variables, with relatively little attention paid to the feedback mechanisms responsible for the evolution of mechanical, rheological and frictional properties. The present study considers these competing feedbacks, focusing on the evolution of the frictional slip weakening rate as a proxy for strengthening and weakening.

Our results are qualitatively compatible with observations made in damage rheology models, that account for distributed plastic deformations and the evolution of the elastic properties of crustal rocks (Lyakhovsky *et al.* 1997a,b, 2001; Hamiel *et al.* 2006). In these studies, the relative efficiency of healing and weakening mechanisms controls the damage distribution and seismic response pattern. In accordance with the damage model of Lyakhovsky *et al.* (2001), we find that fast (slow) healing, implying weak (strong) memory effects of material weakening and slip localization, tends to produce GR (CE) statistics. In our model, different healing rates are modelled using likely variations of the cutoff time t_c , and small and large values of t_c result in GR and CE frequency-size statistics, respectively. The consistency of the results obtained with the two different approaches thus suggests the fundamental role of strength degradation and recovery of material in earthquake source regions.

Studies of granular systems subjected to shear show an evolution of fracture networks (Mora & Place 2002), compatible with the dynamics we observe when weakening dominates in our model. That is, the absence of healing in the granular system causes regions of high shear to remain localized when boundary conditions remain constant. Furthermore, studies on granular materials show that the response of frictional interfaces is highly sensitive to the presence and characteristics of gouge (Place & Mora 1999; Guo & Morgan 2006). While regular stick slip behaviour is typically observed for bare surfaces in laboratory experiments and numerical simulations, gouge filled faults shows highly irregular behaviour. The jostling and rolling of the constituent particles introduces additional degrees of freedom, analogous to fault zone material and gives rise to additional complexity. This highlights the importance of microscopic interactions, which is implicitly considered in the evolution of the slip weakening rate in this study.

5.2 Clustering and mode switching

We observe for a wide range of healing rates fluctuations in the system dynamics and the corresponding frequency-size statistics that are similar to seismicity clustering observed on real faults. Such a situation emerges for $b = 0.02$ and $t_c = 5 \times 10^3$ s (Fig. 8), in which the system exhibits behaviour reminiscent of clustering or mode switching observed in previous studies (Ben-Zion *et al.* 1999). For roughly six loading sequences, our system produces excess large events due to an intermittent development of large- R weakening conditions, which are subsequently suppressed by healing and a decrease of R . Fig. 10(a) illustrates the associated frequency-size distributions for five consecutive time windows with length $2t^*$. The seismicity rate variations for potencies $\log(P) > 0$ are reminiscent of the temporal clustering of palaeoearthquakes on the southern San Andreas fault reported by Biasi *et al.* (2002, and references therein). Biasi *et al.* (2002) doubt, however, that segment interaction is a plausible explanation for clustering at this site because of the

distance to other seismogenic faults. Our approach provides an alternative explanation, that is, frictional properties that evolve on time scales comparable to the sequences in these studies may cause an acceleration and subsequent deceleration of activity.

Seismic clustering, both simulated and observed, need not in general develop the clean characteristics of mode switching observed by Dahmen *et al.* (1998) and Zöller *et al.* (2004) (for observational evidence see Ben-Zion 2008). In the Dahmen *et al.* (1998) and Zöller *et al.* (2004) studies the statistics switch unambiguously between the GR and CE distributions if values of the fixed, time invariant control parameters such as stress loss (i.e. energy lost due to heat or radiated waves) and heterogeneity are in the vicinity of the GR–CE boundary in the stress loss versus heterogeneity plane. In these simulations, the duration of a response type is 10–100 times a loading cycle, and hence several times larger than the time scales associated with the clustering effect (Biasi *et al.* 2002). In contrast to the Dahmen and Zöller mode switching but similar to the present results, Lyakhovsky *et al.* (2001) report mode switching behaviour for time scales of a few cycles, with alternating seismicity patterns that are less distinct than those of Dahmen *et al.* (1998). While the Lyakhovsky *et al.* (2001) damage rheology produces switching seismicity patterns due to changes in the damage, that is, fault distribution, our approach implies similar changes in seismic behaviour due to evolving frictional properties of existing faults. Note that earthquakes in the damage models are not parametrized by frictional instabilities but correspond to sudden irreversible changes in plastic deformation.

5.3 Non-stationarity and predictability

The fluctuations responsible for the clustering effects have implications on the predictability of future events due to incomplete or limited knowledge of past seismicity patterns. Our qualitative analysis reaches the conclusion that feedbacks lower the chance of an accurate estimate of future seismicity occurrence.

The non-stationarity of the dynamics with evolving friction—expressed by significant fluctuations in the dynamics—is apparent by comparing the respective measurements (Figs 8 and 9) to the corresponding results of models with time independent friction (Figs 5 and 6). The corresponding fluctuations in the frequency-size distributions (Fig. 10) also highlight the impact of feedbacks on seismicity evolution. The development of a relatively stable dynamic behaviour of non-evolving systems, illustrated by small to moderate fluctuations of the E and δE measurements around a stable mean, implies a relatively high predictability of future seismicity based on information of past dynamics. In a system dominated by the occurrence of large and very large events (Fig. 8, $R = 2$), fluctuations occur in the course of the seismic cycle, and patterns may exhibit accelerated moment release of medium-size seismicity while the system approaches the punctuation of a large event (Jaumé & Sykes 1999; Zöller & Hainzl 2002). However, anticipations of seismicity rates for time intervals $> 2t^*$ resting on observations of past seismicity are expected to be fairly accurate (Fig. 10a, inset $R = 2$).

In comparison, to assess future behaviour of a system with evolving friction on the basis of past patterns, data from much longer times must be evaluated, due to the increased variability in the dynamics and the associated fluctuations in the frequency-size distributions. Thus, extrapolations based on temporally incomplete information regarding past and recent seismicity possibly over- or underestimate the occurrence of future seismicity, that is, statistics

on observational time scales may not be reliable predictors of future events.

Biased estimates of magnitude dependent occurrence probabilities can also be based on limited sampling from a fixed statistical distribution (Howell 1985; Kagan 1993). That is, the underestimation of the probability of a large event in Howell (1985) is due to incomplete sampling of a hypothetically complete catalogue. However, this mechanism for the variability in event frequency is different from the mechanisms for variability observed in our simulations. Because friction evolution produces statistical distributions that vary with time, the associated variabilities reflect changes in the dynamic regime. In other words, a catalogue that contains the complete seismicity of one cycle may still lead to erroneous estimates of seismicity at later times at which the dynamic regime will have changed.

5.4 Fault zone evolution and organizational principles

5.4.1 Strain organization

The present results show qualitative similarities to models that aim to account for changes of the mechanical properties of crustal material on time scales of fault zone evolution (e.g. Lyakhovsky *et al.* 2001). To balance b -values, that is, the slope, of regional GR statistics, Wesnousky (1999) suggests a co-evolution of fault slip rate and the distribution of faults of a given length. Observations of similar relations, for example, between the number of faults in a network, their lengths, and the average recurrence intervals of fault-size earthquakes, imply a constant adjustment of fault system properties to evolving tectonics. The evolution from initially heterogeneous to longer aligned simpler faults implies the initiation, growth, and coalescence of faults. Simultaneously certain faults from the initial configuration may heal and cease to be active or exhibit decreased seismicity. The evolutionary path associated with growth and coalescence is similar to the 'weakening' trajectory shown in Fig. 9(d). Conversely, the healing and cessation of seismicity, that is, a decrease of fault-size events, is reminiscent of the 'strengthening' trajectory in Fig. 9(d). Furthermore, Wesnousky (1999) discusses that changes in a tectonic regime may lead to the reversal of strain organization, and thus strengthen existing faults and suppress unstable slip.

Strain organization is associated with a tendency to reduce the strain energy (here: E) or configurational entropy more efficiently. This is synonymous with the capability to produce large earthquakes (Main & Burton 1984; Dahmen *et al.* 1998; Al-Kindy & Main 2003). Weakening dominates the formation, structural evolution and geometry of mature earthquake faults. This process has been suggested to follow a global minimization principle (Sornette *et al.* 1994). However, previous approaches do not consider the effects of competing, potentially reversing restrengthening processes, as we do here.

5.4.2 Incremental versus global organization

The process of fault organization, the co-evolution of mechanical and frictional properties, and the corresponding seismicity distributions do not necessarily follow a global optimization strategy to exhibit features reminiscent of an optimized or organized system. Rather, an increase in damage and localization associated with the organization and modification of crustal material—wear and breakage, abrasion, material transport—can result just as easily from local and incremental adjustments, as in the development of other

internally highly structured systems (Carlson & Doyle 2002). The local, incremental evolution of material properties, for example, the smoothing of fault surface topography, as well as the passage of seismic waves and hydrothermal conditions occurs across a range of scales. Fault networks containing mature faults represent structured configurations, incrementally organized for a sufficient release of strain energy for the present tectonic situation. The resulting—even intermittently immature—configurations are not random or disorganized, but represent structures with pronounced history dependence which have evolved to their current state through feedbacks coupling material properties and dynamics.

Local incremental algorithms have been shown to lead to characteristics similar to more globally applied optimization schemes (Carlson & Doyle 2000; Robert *et al.* 2001; Carlson & Doyle 2002; Reynolds *et al.* 2002; Zhou *et al.* 2002). Both global and local algorithms can incorporate feedback and efficiency consistent with a minimization principle. Ultimately, the key feature is that the resulting system is more organized than it is random, so that a description based on organization or optimization, rather than the statistics of an ensemble of random configurations, provides a more accurate starting point for modelling. While we expect biological and technological systems to be much closer to optimal than earthquake faults, the basic consequences of system organization through feedbacks, even at a relatively primitive level, are shown here to have a significant influence on the dynamics.

6 CONCLUSIONS

We conducted numerical experiments on an earthquake fault model to investigate the effect of changes in frictional properties of fault zones on seismicity evolution. The model incorporates empirically observed deformation dependent weakening and competing time dependent healing. Together these control the evolution of the frictional slip weakening rate, R . Time independent, fixed values of R result in GR and CE frequency-size statistics for small and large R , respectively, reflecting frictional properties associated with early and late stages of wear in deformed materials. More complex system dynamics characterized by larger fluctuations in energy measurements result from slip and time dependent changes of the frictional response. That is, slip dependent wear and abrasive mechanisms weaken a frictional interface, but hydrothermal processes are responsible for strength recovery during subsequent at-rest periods. Fast acting healing mechanisms, parametrized by relatively small cutoff times, suppress any tendency in a system for the development of persistent weakening dynamics, whereas for less effective healing the weakening mechanisms dominate. For a broad range of intermediate parameter values, measurements of characteristic quantities exhibit significant fluctuations. The timescale of these fluctuations is large compared to fluctuations in the calibration cases with fixed properties. For simulations with fixed, homogeneous friction data covering relatively short time periods give an accurate measure of the bounds of future seismicity, whereas for simulations with evolving friction the extrapolation of temporally limited past seismicity pattern likely over or underestimates properties of future seismicity.

ACKNOWLEDGMENTS

We thank A. Martin for the outstanding and timely computational assistance that underpinned much of this work. We thank M. L. Manning for a critical in-house review, and comments by Editor C. Ebinger, A. Bizzarri and an anonymous reviewer helped to improve

the manuscript. G. H. was supported by the Swiss National Science Foundation, contribution number PBEZ2-111586, by the James S. McDonnell Foundation, the David and Lucile Packard Foundation, and the NSF under grant DMR-0606092. This research was supported by the Southern California Earthquake Center. SCEC is funded by NSF Cooperative Agreement EAR-0529922 and USGS Cooperative Agreement 07HQAG0008. The SCEC contribution number for this paper is 1190. The Institute for Crustal Studies contribution number for this paper is 0873. Computations were carried out on the 'Dragon' cluster of the Institute for Crustal Studies, University of California, Santa Barbara.

REFERENCES

- Al-Kindy, F.H. & Main, I.G., 2003. Testing self-organized criticality in the crust using entropy: A regionalized study of the CMT global earthquake catalogue, *J. geophys. Res.*, **108**(B11), 2521, doi:10.1029/2002JB002230.
- Andrews, D.J., 2006. Thermal pressurization explains enhanced long-period motion in the Chi-Chi earthquake, *Seism. Res. Lett.*, **77**(2), 264.
- Andrews, D.J. & Ben-Zion, Y., 1997. Wrinkle-like slip pulse on a fault between different materials, *J. geophys. Res.*, **102**(B1), 553–571.
- Antonoli, A., Belardinelli, M.E., Bizzarri, A. & Vogfjord, K.S., 2006. Evidence of instantaneous dynamic triggering during the seismic sequence of year 2000 in south Iceland, *J. geophys. Res.*, **111**, B03302, doi:10.1029/2005JB003935.
- Beeler, N.M., Tullis, T.E., Blanpied, M.L. & Weeks, J.D., 1996. Frictional behavior of large displacement experimental faults, *J. geophys. Res.*, **101**(B4), 8697–8715.
- Ben-Zion, Y., 1996. Stress, slip, and earthquakes in models of complex single-fault systems incorporating brittle and creep deformations, *J. geophys. Res.*, **101**(B3), 5677–5706.
- Ben-Zion, Y., 2001. Dynamic Rupture in recent models of earthquake faults, *J. Mech. Phys. Solids*, **49**, 2209–2244.
- Ben-Zion, Y., 2008. Collective behavior of earthquakes and faults: Continuum-discrete transitions, progressive evolutionary changes and different dynamic regimes, *Rev. Geophys.*, **46**, R94006, doi:10.1029/2008RG000260.
- Ben-Zion, Y. & Lyakhovsky, V., 2006. Analysis of aftershocks in a lithospheric model with seismogenic zone governed by damage rheology, *Geophys. J. Int.*, **165**, 197–210.
- Ben-Zion, Y. & Sammis, C.G., 2003. Characterization of fault zones, *Pure appl. Geophys.*, **160**, 677–715.
- Ben-Zion, Y., Dahmen, K., Lyakhovskiy, V., Ertas, D. & Agnon, A., 1999. Self-driven mode switching of earthquake activity on a fault system, *Earth planet. Sci. Lett.*, **172**, 11–21.
- Ben-Zion, Y., Eneva, M. & Liu, Y., 2003. Large earthquake cycles and intermittent criticality on heterogeneous faults due to evolving stress and seismicity, *J. geophys. Res.*, **108**(B6), 2307, doi:10.1029/2002JB002121.
- Biasi, G.P. II, R.J.W., Fumal, T.E. & Seitz, G.G., 2002. Paleoseismic event dating and the conditional probability of large earthquakes on the southern San Andreas Fault, California, *Bull. seism. Soc. Am.*, **92**(7), 2761–2781.
- Bizzarri, A. & Cocco, M., 2003. Slip-weakening behavior during the propagation of dynamic ruptures obeying rate- and state-dependent friction laws, *J. geophys. Res.*, **108**(B8), doi:10.1029/2002JB002198.
- Bizzarri, A. & Cocco, M., 2006a. A thermal pressurization model for the spontaneous dynamic rupture propagation on a three-dimensional fault: 1. Methodological approach, *J. geophys. Res.*, **111**, doi:10.1029/2005JB003862.
- Bizzarri, A. & Cocco, M., 2006b. A thermal pressurization model for the spontaneous dynamic rupture propagation on a three-dimensional fault: 2. Traction evolution and dynamic parameters, *J. geophys. Res.*, **111**, doi:10.1029/2005JB003864.
- Blanpied, M.L., Marone, C.J., Lockner, D.A., Byerlee, J.D. & King, D.P., 1998. Quantitative measure of the variation in fault rheology due to fluid-rock interactions, *J. geophys. Res.*, **103**(B5), 9691–9712.
- Bosl, W.J. & Nur, A., 2002. Aftershocks and pore fluid diffusion following the 1992 Landers earthquake, *J. geophys. Res.*, **107**(B12), 2366, doi:10.1029/2001JB000155.
- Burridge, R. & Knopoff, L., 1967. Model and theoretical seismicity, *Bull. seism. Soc. Am.*, **57**(3), 341–371.
- Byerlee, J.D., 1978. Friction of rock, *Pure appl. Geophys.*, **116**, 615–626.
- Byerlee, J.D., 1990. Friction, overpressure and fault normal compression, *Geophys. Res. Lett.*, **17**(12), 2109–2112.
- Carlson, J.M., 1991. Time intervals between characteristic earthquakes and correlations with smaller events: An analysis based on a mechanical model of a fault, *J. geophys. Res.*, **96**(B3), 4255–4267.
- Carlson, J.M. & Doyle, J., 2000. Highly Optimized tolerance: Robustness and design in complex systems, *Phys. Rev. Lett.*, **84**(11), 2529–2532.
- Carlson, J.M. & Doyle, J., 2002. Complexity and robustness, *Proc. Natl. Acad. Sci. USA*, **99**, 2538–2545.
- Carlson, J.M. & Langer, J.S., 1989a. Properties of earthquakes generated by fault dynamics, *Phys. Rev. Lett.*, **62**(22), 2632–2635.
- Carlson, J.M. & Langer, J.S., 1989b. Mechanical model of an earthquake fault, *Phys. Rev. A*, **40**(11), 6470–6484.
- Carlson, J.M., Langer, J.S., Shaw, B.E. & Tang, C., 1991. Intrinsic properties of a Burridge-Knopoff model of an earthquake fault, *Phys. Rev. A*, **44**(2), 884–897.
- Carlson, J.M., Langer, J.S. & Shaw, B.E., 1994. Dynamics of earthquake faults, *Rev. Mod. Phys.*, **66**(2), 657–670, Colloquium Paper.
- Chambon, G., Schmittbuhl, J. & Corfdir, A., 2006. Frictional response of a thick gouge sample: 1. Mechanical measurements and microstructures, *J. geophys. Res.*, **111**, B09308, doi:10.1029/2003JB002731.
- Chester, F.M. & Chester, J.S., 1998. Ultracataclastic structure and friction processes of the Punchbowl Fault, San Andreas System, California, *Tectonophysics*, **295**, 199–221.
- Chester, F.M., Chester, J.S., Kirschner, D.L., Schulz, S.E. & Evans, J.P., 2004. Structure of large-displacement, strike-slip fault zones in the brittle continental crust, in *Rheology and Deformation in the Lithosphere at Continental Margins*, pp. 223–260, eds Karner, G.D., Taylor, B., Driscoll, N.W. & Kohlstedt, D.L., Columbia University Press, New York.
- Cowie, P.A. & Scholz, C.H., 1992. Physical explanation for the displacement-length relationship of faults using a post-yield fracture mechanics model, *J. Struct. Geol.*, **14**, 1133–1148.
- Dahmen, K., Ertas, D. & Ben-Zion, Y., 1998. Gutenberg-Richter and characteristic earthquake behavior in simple mean field models of heterogeneous faults, *Phys. Rev. E*, **58**(2), 1494–1501.
- Daub, E.G. & Carlson, J.M., 2008. A constitutive model for fault gouge deformation in dynamic rupture simulations, *J. geophys. Res.*, **113**, B12309, doi:10.1029/2007JB005377.
- Dieterich, J.H., 1972. Time-dependent friction in rocks, *J. geophys. Res.*, **77**(20), 3690–3697.
- Dieterich, J.H., 1978. Time-dependent friction and the mechanics of stick-slip, *Pure appl. Geophys.*, **116**, 790–805.
- Dieterich, J.H., 1992. Earthquake nucleation on faults with rate- and state-dependent strength, *Tectonophysics*, **211**, 115–134.
- Dieterich, J.H. & Kilgore, B.D., 1994. Direct observation of frictional contacts: New insights for state-dependent properties, *Pure appl. Geophys.*, **143**(1/2/3), 283–302.
- Falk, M.L. & Langer, J.S., 1998. Dynamics of viscoplastic deformation in amorphous solids, *Phys. Rev. E*, **57**, 7192–7205.
- Falk, M.L. & Langer, J.S., 2000. From simulation to theory in the physics of deformation and fracture, *M.R.S. Bull.*, **25**(40).
- Fialko, Y., 2004. Probing the mechanical properties of seismically active crust with space geodesy: Study of coseismic deformation due to the 1992 M_w 7.3 Landers (southern California) earthquake, *J. geophys. Res.*, **109**, B03307, doi:10.1029/2003JB002756.
- Fialko, Y., 2006. Interseismic strain accumulation and the earthquake potential on the southern San Andreas fault system, *Nature*, **441**, 968–971.
- Fisher, D.S., Dahmen, K., Ramanathan, S. & Ben-Zion, Y., 1997. Statistics of earthquakes in simple models of heterogeneous faults, *Phys. Rev. Lett.*, **78**(25), 4885–4888.
- Fu, X.-Y., Kasai, T., Falk, M.L. & Rigney, D.A., 2001a. Sliding behavior of metallic glass Part I. Experimental investigations, *WEAR*, **250**, 409–419.

- Fu, X.-Y., Kasai, T., Falk, M.L. & Rigney, D.A., 2001b. Sliding behavior of metallic glass Part II. Computer simulations, *WEAR*, **250**, 420–430.
- Gu, J.-C., Rice, J.R., Ruina, A.L. & Tse, S.T., 1984. Slip motion and stability of a single degree of freedom elastic system with rate and state dependent friction, *J. Mech. Phys. Solids*, **32**, 167–196.
- Gu, Y. & Wong, T.-F., 1994. Development of Shear localization in simulated quartz gouge: Effect of cumulative slip and gouge particle size, *Pure appl. Geophys.*, **143**(1/2/3), 387–423.
- Guo, Y. & Morgan, J.K., 2004. Influence of normal stress and grain shape on granular friction: Results of discrete element simulations, *J. geophys. Res.*, **109**, B12305, doi:10.1029/2004JB003044.
- Guo, Y. & Morgan, J.K., 2006. The frictional and micromechanical effects of grain comminution in fault gouge from distinct element simulations, *J. geophys. Res.*, **111**, B12406, doi:10.1029/2005JB004049.
- Guo, Y. & Morgan, J.K., 2007. Fault gouge evolution and its dependence on normal stress and rock strength—results of discrete element simulations: gouge zone properties, *J. geophys. Res.*, **111**, B10403, doi:10.1029/2006JB004524.
- Hamiel, Y., Katz, O., Lyakhovsky, V., Reches, Z. & Fialko, Y., 2006. Stable and unstable damage evolution in rocks with implications to fracturing of granite, *Geophys. J. Int.*, **167**, 1005–1016.
- Heimpel, M.H., 2003. Characteristic scales of earthquake rupture from numerical models, *Nonlin. Proc. Geophys.*, **10**(6), 573–584.
- Hickman, N.M.B.S.H. & Wong, T.-F., 2001. Earthquake stress drop and laboratory-inferred interseismic strength recovery, *J. geophys. Res.*, **106**, 30 701–30 713.
- Hickman, S., Sibson, R. & Bruhn, R., 1995. Introduction to special section: Mechanical involvement of fluids in faulting, *J. geophys. Res.*, **100**(B7), 12 831–12 840.
- Hill, P. et al., 1993. Seismicity remotely triggered by the magnitude 7.3 Landers, California, Earthquake, *Science*, **260**(5114), 1617–1623.
- Hillers, G., Ben-Zion, Y. & Mai, P.M., 2006. Seismicity on a fault with rate- and state-dependent friction and spatial variations of the critical slip distance, *J. geophys. Res.*, **111**, B01403, doi:10.1029/2005JB003859.
- Hillers, G., Mai, P.M., Ben-Zion, Y. & Ampuero, J.P., 2007. Statistical properties of seismicity of fault zones at different evolutionary stages, *Geophys. J. Int.*, **169**, 515–533.
- Hiramatsu, Y., Honma, H., Saiga, A., Furumoto, M. & Ooida, T., 2005. Seismological evidence on characteristic time of crack healing in the shallow crust, *Geophys. Res. Lett.*, **32**, L09304, doi:10.1029/2002GL022657.
- Hong, T.-K. & Menke, W., 2006. Tomographic investigation of the wear along the San Jacinto fault, southern California, *Phys. Earth planet. Inter.*, **155**, 236–248.
- Howell, B.F., 1985. On the effect of too small a data base on earthquake frequency diagrams, *Bull. seism. Soc. Am.*, **75**(4), 1205–1207.
- Husen, S., Taylor, R., Smith, R.B. & Healsler, H., 2004. Changes in geyser eruption behavior and remotely triggered seismicity in Yellowstone National Park produced by the 2002 M 7.9 Denali fault earthquake, Alaska, *Geology*, **32**(6), 537–540.
- Ida, Y., 1972. Cohesive force across the tip of a longitudinal-shear crack and Griffith's specific surface energy, *J. geophys. Res.*, **94**(B4), 4089–4104.
- Jaumé, S.C. & Sykes, L.R., 1999. Evolving towards a critical point: A review of accelerating seismic moment/energy release prior to large and great earthquakes, *Pure appl. Geophys.*, **155**, 279–306.
- Kagan, Y.Y., 1993. Statistics of characteristic earthquakes, *Bull. seism. Soc. Am.*, **83**(1), 7–24.
- Kim, J., 2006. Emergence: Core ideas and issues, *Synthese*, **151**, 547–559.
- Langer, J.S., 2008. Shear-transformation-zone theory of plastic deformation near the glass transition, *Phys. Rev. E*, **77**, 021502.
- Langer, J.S. & Manning, M.L., 2007. Steady-state, effective-temperature dynamics in a glassy material, *Phys. Rev. E*, **76**, 056107.
- Langer, J.S., Carlson, J.M., Myers, C.R. & Shaw, B.E., 1996. Slip complexity in dynamic models of earthquake faults, *Proc. Natl. Acad. Sci. USA*, **93**, 3825–3829, Colloquium Paper.
- Lapusta, N., Rice, J.R., Ben-Zion, Y. & Zheng, G., 2000. Elastodynamic analysis for slow tectonic loading with spontaneous rupture episodes on faults with rate- and state-dependent friction, *J. geophys. Res.*, **105**(B10), 23 765–23 789.
- Lee, A.G.G. & Rutter, E.H., 2004. Experimental rock-on-rock frictional wear: Application to subglacial abrasion, *J. geophys. Res.*, **109**, B09202, doi:10.1029/2004JB003059.
- Li, Y.-G., Chen, P., Cochran, E.S., Vidale, J.E. & Burdette, T., 2006. Seismic evidence for rock damage and healing on the San Andreas Fault Associated with the 2004 M6.0 Parkfield Earthquake, *Bull. seism. Soc. Am.*, **96**(4B), S349–S363.
- Liu, Y. & Rice, J.R., 2007. Spontaneous and triggered aseismic deformation transients in a subduction fault model, *J. geophys. Res.*, **112**, B09404, doi:10.1029/2007JB004930.
- Lockner, D.A. & Byerlee, J.D., 1993. How geometrical constraints contribute to the weakness of mature faults, *Nature*, **363**, 250–252.
- Lockner, D.A. & Byerlee, J.D., 1994. Dilatancy in hydraulically isolated faults and the suppression of instability, *Geophys. Res. Lett.*, **21**(22), 2353–2356.
- Lockner, D.A., Byerlee, J.D., Kuksenko, V., Ponomarev, A. & Sidorin, A., 1991. Quasi-static fault growth and shear fracture energy in granite, *Nature*, **350**, 39–42.
- Lois, G., Lemaître, A. & Carlson, J.M., 2005. Numerical tests of constitutive laws for dense granular flows, *Phys. Rev. E*, **72**(5), 051303.
- Lyakhovsky, V., Ben-Zion, Y. & Agnon, A., 1997a. Distributed damage, faulting, and friction, *J. geophys. Res.*, **102**(B12), 27 635–27 649.
- Lyakhovsky, V., Reches, Z., Weinberger, R. & Scott, T.E., 1997b. Non-linear elastic behavior of damaged rocks, *Geophys. J. Int.*, **130**, 157–166.
- Lyakhovsky, V., Ben-Zion, Y. & Agnon, A., 2001. Earthquake cycle, fault zones, and seismicity patterns in a rheologically layered lithosphere, *J. geophys. Res.*, **106**(B3), 4103–4120.
- Main, I.G. & Burton, P.W., 1984. Information theory and the earthquake frequency-magnitude distribution, *Bull. seism. Soc. Am.*, **74**(4), 1409–1426.
- Maloney, C.E. & Lemaître, A., 2006. Amorphous systems in athermal, quasistatic shear, *Phys. Rev. E*, **74**, 016118.
- Manning, M.L., Langer, J.S. & Carlson, J.M., 2007. Strain localization in a shear transformation zone model for amorphous solids, *Phys. Rev. E*, **76**, 056106.
- Marone, C., 1998. Laboratory-derived friction laws and their application to seismic faulting, *Annu. Rev. Earth planet. Sci.*, **26**, 643–696.
- Marone, C. & Kilgore, B., 1993. Scaling of the critical slip distance for seismic faulting with shear strain in fault zones, *Nature*, **362**, 618–621.
- Marone, C., Vidale, J.E. & Ellsworth, W.L., 1995. Fault healing inferred from time dependent variations in source properties of repeating earthquakes, *Geophys. Res. Lett.*, **22**(22), 3095–3098.
- Mehta, A.P., Dahmen, K.A. & Ben-Zion, Y., 2006. Universal mean moment rate profiles of earthquake ruptures, *Phys. Rev. E*, **73**, 056104.
- Miller, S.A., 2006. Fluid-Controlled Aftershock Patterns from Different Tectonic Regimes, *EOS, Trans. Am. geophys. Un.*, **87**(52), Fall. Meet. Suppl., Abstract T12A-08.
- Miller, S.A., Collettini, C., Chiaraluce, L., Cocco, M., Barchi, M. & Kaus, J.P., 2004. Aftershocks driven by a high-pressure CO₂ source at depth, *Nature*, **427**, 724–727.
- Mora, P. & Place, D., 1999. The weakness of earthquake faults, *Geophys. Res. Lett.*, **26**(1), 123–126.
- Mora, P. & Place, D., 2002. Stress Correlation function evolution in lattice solid elasto-dynamic models of shear and fracture zones and earthquake prediction, *Pure appl. Geophys.*, **159**, 2413–2427.
- Morgan, J.K. & Boettcher, M.S., 1999. Numerical simulations of granular shear zones using the distinct element method I. Shear zone kinematics and the micromechanics of localization, *J. geophys. Res.*, **104**(B2), 2703–2719.
- Nakatani, M. & Scholz, C.H., 2004. Frictional healing of quartz gouge under hydrothermal conditions: 1. Experimental evidence for solution transfer healing mechanism, *J. geophys. Res.*, **109**, B07201, doi:10.1029/2001JB001522.
- Nakatani, M. & Scholz, C.H., 2006. Intrinsic and apparent short-time limits for fault healing: Theory, observations, and implications for velocity-dependent friction, *J. geophys. Res.*, **111**, B12208, doi:10.1029/2005JB004096.

- Niemeijer, A.R. & Spiers, C.J., 2006. Velocity dependence of strength and healing behaviour in simulated phyllosilicate-bearing fault gouge, *Tectonophysics*, **427**, 231–253.
- Nur, A. & Booker, J.R., 1972. Aftershocks caused by pore fluid flow? *Science*, **175**, 885–887.
- Ohnaka, M., 2003. A constitutive scaling law and a unified comprehension for frictional slip failure, shear fracture of intact rock, and earthquake rupture, *J. geophys. Res.*, **108**(B2), 2080, doi:10.1029/2000JB000123.
- Ord, A., Hobbs, B. & Regenauer-Lieb, K., 2007. Shear band emergence in granular materials—a numerical study, *Int. J. Numer. Anal. Methods Geomech.*, **31**, 373–393.
- Passchier, C.W. & Trouw, R.A.J. (eds), 2005. *Microtectonics*, 2nd edn, Springer, Berlin.
- Perfettini, H., Campillo, M. & Ionescu, I., 2003. On the scaling of the slip weakening rate of heterogeneous faults, *J. geophys. Res.*, **108**(B9), 2410, doi:10.1029/2002JB001969.
- Piombo, A., Martinelli, G. & Dragoni, M., 2005. Post-seismic fluid flow and Coulomb stress changes in a poroelastic medium, *Geophys. J. Int.*, **162**, 507–515.
- Place, D. & Mora, P., 1999. The lattice solid model to simulate the physics of rocks and earthquakes: Incorporation of friction, *J. Comp. Phys.*, **150**, 332–372.
- Power, W.L., Tullis, T.E. & Weeks, J.D., 1988. Roughness and wear during brittle failure, *J. geophys. Res.*, **93**, 15 268–15 278.
- eds Press, W.H., Teukolsky, S.A., Vetterling, W.T. & Flannery, B.P., 1992. *Numerical Recipes in FORTRAN: The Art of Scientific Computing*, 2nd edn, Cambridge Univ. Press, Cambridge.
- Rempel, A.W. & Rice, J.R., 2006. Thermal pressurization and onset of melting in fault zones, *J. geophys. Res.*, **111**, B09314, doi:10.1029/2006JB004314.
- Reynolds, D., Carlson, J.M. & Doyle, J., 2002. Design degrees of freedom and mechanisms for complexity, *Phys. Rev. E*, **66**(1), 016108.
- Rice, J.R., 1992. Fault stress states, pore pressure distributions, and the weakness of the San Andreas Fault, in *Fault Mechanics and Transport Properties in Rocks*, pp. 475–503, eds Evans, B. & Wong, T.-F., Academic Press, San Diego, CA.
- Rice, J.R., 1993. Spatio-temporal complexity of slip on a fault, *J. geophys. Res.*, **98**(B6), 9885–9907.
- Rice, J.R., 2006. Heating and weakening of faults during earthquake slip, *J. geophys. Res.*, **111**, B05311, doi:10.1029/2005JB004006.
- Rice, J.R. & Gu, J.-C., 1983. Earthquake aftereffects and triggered seismic phenomena, *Pure appl. Geophys.*, **121**(2), 187–219.
- Rice, J.R. & Ruina, A.L., 1983. Stability of steady frictional slipping, *J. Appl. Mech.*, **50**, 343–349.
- Richardson, E. & Marone, C., 1999. Effect of normal stress vibrations on frictional healing, *J. geophys. Res.*, **104**(B12), 28 859–28 878.
- Robert, C., Carlson, J.M. & Doyle, J., 2001. Highly optimized tolerance in epidemic models incorporating local optimization and regrowth, *Phys. Rev. E*, **63**(5), 056122.
- Rubin, A.M. & Ampuero, J.-P., 2005. Earthquake nucleation on (aging) rate and state faults, *J. geophys. Res.*, **110**, B11312, doi:10.1029/2005JB003686.
- Ruina, A., 1983. Slip instability and state variable friction laws, *J. geophys. Res.*, **88**(B12), 10 359–10 370.
- Sammis, C.G. & Sornette, D., 2002. Positive feedback, memory, and the predictability of earthquakes, *Proc. Natl. Acad. Sci. USA*, **99**, 2501–2508, Colloquium Paper, doi:10.1073/pnas.012580999.
- Scholz, C.H. (ed.), 1990. *The Mechanics of Earthquakes and Faulting*, 1st edn, Cambridge University Press, Cambridge.
- Segall, P. & Rice, J.R., 1995. Dilatancy, compaction, and slip instability of a fluid-infiltrated fault, *J. geophys. Res.*, **100**(B11), 22 155–22 171.
- Segall, P. & Rice, J.R., 2006. Does shear heating of pore fluid contribute to earthquake nucleation? *J. geophys. Res.*, **111**, B09316, doi:10.1029/2005JB004129.
- Shaw, B.E. & Rice, J.R., 2000. Existence of continuum complexity in the elastodynamics of repeated fault ruptures, *J. geophys. Res.*, **105**(B10), 23 791–23 810.
- Shibazaki, B., 2005. Nucleation process with dilatant hardening on a fluid-infiltrated strike-slip fault model using a rate- and state-dependent friction law, *J. geophys. Res.*, **110**, B11308, doi:10.1029/2005JB003741.
- Sibson, R.H., 1980. Transient discontinuities in ductile shear zones, *J. Struct. Geol.*, **2**(1/2), 165–171.
- Sibson, R.H., 2007. An episode of fault-valve behavior during compressional inversion?—the 2004 *M*_J6.8 Mid-Niigata Prefecture, Japan, earthquake sequence, *Earth planet. Sci. Lett.*, **257**, 188–199.
- Sleep, N.H. & Blanpied, M.L., 1992. Creep, compaction and the weak rheology of major faults, *Nature*, **359**, 687–692.
- Sornette, D., Miltenberger, P. & Vanneste, C., 1994. Statistical physics of fault patterns self-organized by repeated earthquakes, *Pure appl. Geophys.*, **142**, 491–527.
- Stirling, M.W., Wesnousky, S.G. & Shimazaki, K., 1996. Fault Trace complexity, cumulative slip, and the shape of the magnitude-frequency distribution for strike-slip faults: A global survey, *Geophys. J. Int.*, **124**, 833–868.
- Tenthorey, E. & Cox, S.F., 2006. Cohesive strengthening of fault zones during the interseismic period: An experimental study, *J. geophys. Res.*, **111**, B09202, doi:10.1029/2005JB004122.
- Toro, G.D., Goldsby, D.L. & Tullis, T.E., 2004. Friction falls towards zero in quartz rock as slip velocity approaches seismic rates, *Nature*, **427**, 436–439.
- Vidale, J.E., Ellsworth, W.L., Cole, A. & Marone, C., 1994. Variations in rupture process with recurrence interval in a repeated small earthquake, *Nature*, **368**, 624–626.
- Wang, W. & Scholz, C.H., 1994. Wear processes during frictional sliding of rock: A theoretical and experimental study, *J. geophys. Res.*, **99**(B4), 6789–6799.
- Weatherley, D., Mora, P. & Xia, M.F., 2002. Long-range automaton models of earthquakes: Power-law accelerations, correlation evolution, and mode-switching, *Pure appl. Geophys.*, **159**, 2469–2490.
- Wesnousky, S.G., 1988. Seismological and structural evolution of strike-slip faults, *Nature*, **335**, 340–343.
- Wesnousky, S.G., 1994. The Gutenberg-Richter or characteristic earthquake distribution. Which is it?, *Bull. seism. Soc. Am.*, **84**(6), 1940–1959.
- Wesnousky, S.G., 1999. Crustal deformation processes and the stability of the Gutenberg-Richter relationship, *Bull. seism. Soc. Am.*, **89**(4), 1131–1137.
- Wilson, J.E., Chester, J.S. & Chester, F.M., 2003. Microfracture analysis of fault growth and wear processes, Punchbowl Fault, San Andreas system, California, *J. Struct. Geol.*, **25**, 1855–1873.
- Xia, J., Gould, H., Klein, W. & Rundle, J.B., 2005. Simulations of the Burridge-Knopoff model of earthquakes with variable range stress transfer, *Phys. Rev. Lett.*, **95**(24), 248501.
- Yasuhara, H., Marone, C. & Ellsworth, D., 2005. Fault zone restrengthening and frictional healing: The role of pressure solution, *J. geophys. Res.*, **110**, B06310, doi:10.1029/2004JB003327.
- Zhou, T., Carlson, J.M. & Doyle, J., 2002. Mutation, specialization, and hypersensitivity in highly optimized tolerance, *Proc. Natl. Acad. Sci. USA*, **99**(4), 2049–2054.
- Zöller, G. & Hainzl, S., 2002. A systematic spatiotemporal test of the critical point hypothesis for large earthquakes, *Geophys. Res. Lett.*, **29**, 1558, doi:10.1029/2002GL014856.
- Zöller, G., Holschneider, M. & Ben-Zion, Y., 2004. Quasi-static and quasi-dynamic modeling of earthquake failure at intermediate scales, *Pure appl. Geophys.*, **161**, 2103–2118.
- Zöller, G., Holschneider, M. & Ben-Zion, Y., 2005. The role of heterogeneities as a tuning parameter of earthquake dynamics, *Pure appl. Geophys.*, **162**, 1027–1049.

APPENDIX

Here we discuss in more detail a variety of physical mechanisms that may influence weakening and strengthening on faults. Our model is sufficiently general to be at least qualitatively consistent with a range of possible mechanisms discussed here.

During the process of strain organization the micro- and macromechanical properties of the involved materials constantly change. These changes affect the stability and dynamics of earthquake faults. The complex multiscale interactions of the competing weakening and strengthening processes suggest that homogeneous, time independent properties are unlikely to adequately describe the state of fault systems and individual faults. While this seems trivial for time scales spanning the dimensions of fault zone formation and development within stable tectonic boundary conditions, mechanisms that change the microstates of frictional interfaces imply that equilibrated conditions are similarly unlikely to be met during shorter time periods. The purpose of this Appendix is to illustrate the breadth of physical processes which may be relevant.

A1 Overview

Despite the limited capability to meet conditions at several kilometers depth in laboratory experiments, studies of rock deformation reproduce certain aspects of fault zone formation. Acoustic emissions reveal that initially formed microcracks coalesce to form slip surfaces, and during this process material properties change significantly in response to irreversible deformations. Despite the wide range of possible and occasionally contradictory responses of crustal material to external forcing—depending on locally variable conditions such as mineral composition, the abundance and phase of fluids, and temperature gradients—fault (system) development can conceptually be characterized by the following sequence. (1) The rheologic weakening of initially intact though probably heterogeneous rock. (2) The localization of deformation accompanied by the regularization of geometric heterogeneities. (3) Abrasive mechanisms and wear produce a widening process zone around fault cores, and the formed gouges control the frictional response to forcing. (4) Geometric complexities continuously lead to irregularly distributed places of wear and material accumulation.

The development of mature faults, and the adjustment of fault geometries to changes in the tectonic regime expressed by the simultaneous formation of younger structures indicate that properties of regional fault systems change. That is, although mature faults (e.g. the San Andreas fault) accommodate significant portions of relative plate motion, immature faults (e.g. the San Jacinto fault) form in close proximity because the stress field favours strain release in these areas associated with a higher degree of energy dissipation. While fault zone formation and evolution operates on time scales of the order of 10^3 – 10^5 yr—at least ten times the cycle duration of large earthquakes—material properties might change over times as small as milliseconds, associated with earthquake rupture propagation.

A2 Friction

Our model investigates changes in friction behaviour due to weakening and strengthening feedbacks. This subsection discusses additional evidence that support the sensitivity of the friction evolution on microscopic conditions.

Rock friction assumes the existence of a sliding surface that may have formed during a breakup process as described above. The leading order static friction coefficient has been found to be independent of rock type (Byerlee 1978). However, the evolution of the frictional resistance during instabilities controls the behaviour of earthquake faults, and has been observed to depend on existence, composition and characteristics of gouge, normal stresses, existence

of fluids, chemical composition, deformation history, hydrothermal conditions, interevent hold times and strain and slip rates. Experiments on dry, bare surfaces at room temperature show an inverse proportionality between sliding friction and slip rates (Niemeijer & Spiers 2006, and references therein). Details of friction evolution depend on the roughness of the sliding surfaces, which controls the evolution distance in the rate-and-state framework (Dieterich 1972, 1978), correlating smooth and rough surfaces with effective weakening and strengthening behaviour, respectively. A large body of theoretical and numerical work discusses the effects of occasionally subtle changes in the constitutive rate-and-state parameters on system stability (e.g. Ruina 1983; Rice & Gu 1983; Rice & Ruina 1983; Gu *et al.* 1984; Dieterich 1992; Rubin & Ampuero 2005).

The rate-and-state formulation has been shown to be applicable over a range of quasi-static slip speeds to friction of bare surfaces and the gouge layer, which exhibits a broader response spectrum. Successive wear of contact asperities leads to the formation of gouge (Power *et al.* 1988; Wang & Scholz 1994; Beeler *et al.* 1996). According to Lockner & Byerlee (1993) and Beeler *et al.* (1996), the gouge remains localized exhibiting weakening properties as long as the shear failure strength remains lower than the strength of the surroundings. Beeler *et al.* (1996) observed in rotary shear experiments of initially bare surfaces an overall velocity weakening, that is interrupted by a period of strengthening behaviour. Continued wear results in a widening of the gouge zone (Power *et al.* 1988; Gu & Wong 1994; Marone 1998), and its stability sensitively depends on multiple factors. Furthermore, gouge composed of mixtures behaves different from homogeneous materials (Niemeijer & Spiers 2006).

Experimental studies have revealed the critical role of fluids in gouge filled faults (see references in Niemeijer & Spiers 2006), and theoretical studies demonstrated that dilatant gouges under wet conditions can develop properties that suppress unstable slip (e.g. Segall & Rice 1995). A successive organization of material in the fault core possibly leads to hydraulically and thermally isolated structures, that give rise to rapid weakening mechanisms (e.g. Andrews 2006; Rice 2006; Segall & Rice 2006). Although relatively rare, molten material as a result of high slip speeds and thermal isolation (Sibson 1980; Passchier & Trouw 2005; Rempel & Rice 2006; Rice 2006; Bizzarri & Cocco 2006a,b) might further contribute to the formation of spatially heterogeneous fault strength in the aftermath of large slip events.

Common to all laboratory rock experiments is the limitation to relatively small total offsets without bringing the same material in contact over and over again, and the use of relatively straight and planar frictional surfaces or gouge geometries. Furthermore, experiments fail to combine coseismic high slip rates, large displacements and normal stresses associated with crustal dynamic faulting events (Toro *et al.* 2004). Consequently, most measurements show an initial transient followed by a steady state response (Lee & Rutter 2004). Whereas first order friction effects can be observed analysing these experiments, important aspects of geometrical heterogeneity cannot be addressed.

A3 Granular materials

As briefly discussed in Section 5, observations of the highly sensitive and non-linear dynamics associated with granular materials have important implications for fault zone stability. The notion that fault zone gouge consists of microscopic particles suggests granular materials subject to shear strain may be a proxy

of earthquake fault behaviour. Furthermore, the granular approach to study the evolution of dynamic variables is supported by the occurrence of discontinuities in the crust, that is, surfaces within broken material unaffected by healing (Ben-Zion & Sammis 2003). These two observations indicate that the applicability of a discrete, granular approach depends on the scale of the phenomena under investigation.

Ord *et al.* (2007) discusses the advantage of a discrete particle approach over continuum descriptions to investigate emergent phenomena (Kim 2006) in geomaterials, including fracture evolution and strain localization. In numerical studies of granular systems, simple atomic-bond-like interactions permit the evolution of patterning such as shear bands. Recent work by Langer & Manning (2007) and Langer (2008) has shown, however, that continuum models spontaneously develop shear bands as well. In these continuum models, strain softening emerges naturally from a mean-field description of the microscopic dynamics, in contrast to typical plasticity models where the softening is included only phenomenologically. According to the underlying Shear Transformation Zone (STZ) theory (Falk & Langer 1998, 2000), microscopic configurational rearrangements within the gouge occur much more slowly than macroscopic stress equilibration, suggesting a mechanism for the continued change of a gouge state over long time scales (Manning *et al.* 2007). Applying the theory within an elastodynamic framework, Daub & Carlson (2008) showed that small differences in shear strain localization influences the nucleation, propagation, and arrest of elastodynamic ruptures and can thus lead to drastically different results for earthquake simulations.

Granular systems subject to shear develop strongly anisotropic time dependent stress fields (Mora & Place 2002; Maloney & Lemaître 2006; Ord *et al.* 2007), where force chains carry most of the applied load. Furthermore, the relative abundance of different grain shapes within synthetic gouge has strong implications on its stability (Guo & Morgan 2004). Continuous grain comminution affects gouge zone features and thus mechanical properties of fault zones, thereby affecting fault strength and stability (Mora & Place 1999; Guo & Morgan 2006). Spatially variable properties of gouges persist in geometrically simpler fault configurations, resulting in changes of microscopic states even though macroscopically a steady state can be approached (Morgan & Boettcher 1999; Lois *et al.* 2005). Guo & Morgan (2007) discuss the generally poorly constrained progressive change of granular gouge properties, and observe in their numerical experiment that neither gouge zone thickness nor grain size distribution evolve to a steady state value.

Wear and surface evolution are also reported in shear experiments of non-geomaterials (e.g. Fu *et al.* 2001a), leading to heterogeneous surface alteration and continued abrasion of non-planar obstacles. Accompanying molecular dynamics simulations (Fu *et al.* 2001b) demonstrate the importance of mixing phenomena at all stages of sliding. While Chester & Chester (1998) did not observe mixed material in the fault core during late stages of faulting, competing processes of debris formation and removal by wear are likely to play a significant role in early and intermediate stages of fault zone evolution.

A4 Mechanical properties of evolving fault zones

Since the evolution of friction is the focus of the present study, mechanical properties of the material surrounding faults—represented by the loader spring stiffness k_p (Fig. 1b) in our model—are not discussed. However, changes in the mechanical properties significantly

influence the stability of faults, for example, due to differences in stress buildup and unloading.

The dominant deformation mechanism in relatively young faults is the creation of damaged and broken material through fracturing and comminution. Competing processes such as wear, abrasion and the smoothing effects of debris removal tend to decrease structural irregularities. Analysis of exhumed fault sections from mid-crustal depths indicate that slip localizes on a relatively narrow zone early in the development, during a stage in which a considerable amount of geometrical complexity still prevails (Chester & Chester 1998; Chester *et al.* 2004, and references therein). Yield strength and related mechanical rock properties evolve during continued deformation from values of intact rock to the frictional resistance of highly localized shear zones (Cowie & Scholz 1992).

Although structurally simpler, mature faults show roughness at larger scales and wavelengths, and become never perfectly planar and homogeneous. Even very small geometric heterogeneity has strong implications on peak stresses and relaxation at fault irregularities (J. Dieterich, SCEC Earthquake Simulators Workshop, 2008). Continued displacement along non-planar surfaces results in local stress concentrations responsible for episodic reloading of rocks passing irregularities (Wilson *et al.* 2003). Wrinkle-like slip pulses associated with rupture along bimaterial interfaces brought into contact as a result of large cumulative offsets (Andrews & Ben-Zion 1997), and the accompanied passage of a rupture tip may also contribute to the accumulation of asymmetric damage patterns. Thus local material properties in the vicinity of a fault are continuously altered (Chester & Chester 1998).

Hong & Menke (2006) estimate the spatial dimension of a wear related zone of the San Jacinto fault and concluded that it extends to depths of the brittle–ductile transition zone, indicating its mechanical importance throughout the seismogenic depth. The analysis of fault zone trapped waves allows the estimate of *in situ* large scale wear processes, revealing the existence of a highly fractured zone around the fault core. This low velocity zone, typically a few hundred meters to 1 km wide, persists around large offset faults, consistent with observations from exhumed fault segments. Spatially variable and asymmetric rigidity gradients between intact host rocks and the damaged material (Fialko 2006; Li *et al.* 2006), and the spatiotemporal variation in strength of strongly deformable low-rigidity compliant zones (Fialko 2004) likely influence the seismic response in an irregular manner. The rheology of damaged rocks differs in fundamental ways from the reversible deformation associated with Hookean elasticity. Experiments on the response beyond the elastic, linear portion reveal the irreversible change in material properties of highly deformed rock (e.g. Lockner *et al.* 1991), and are attributed to the density and distribution of microcracks. Continued cyclic loading progressively increases the yield stress at the onset of damage, whereas the material strength decreases with accumulated damage (Hamiel *et al.* 2006). Permanently deformed rocks dominate crustal properties particularly in tectonically and thus seismically active regions, and the evolving non-linear response to changing stress states likely influences regional seismicity pattern (e.g. Ben-Zion & Lyakhovsky 2006).

A5 The role of fluids

Fluid assisted processes are implicitly assumed in our model by applying variations in the cutoff time t_c observed by Nakatani & Scholz (2004) conducting fluid saturated friction experiments. The existence and properties of fluid phases in the seismogenic

crust, and their effect on fault stability is in general hard to constrain.

Hence, fluids play an important but not well understood role in the earthquake process (Hickman *et al.* 1995, and references therein). Observational evidence relates fluids to a variety of faulting phenomena, such as fluid driven aftershocks (Nur & Booker 1972; Bosl & Nur 2002; Miller *et al.* 2004; Piombo *et al.* 2005), remotely triggered earthquakes (Hill *et al.* 1993; Husen *et al.* 2004; Antonioli *et al.* 2006), generation of aseismic transients, tremors and possibly silent slip events (Segall & Rice 1995; Shibazaki 2005; Liu & Rice 2007). Laboratory experiments investigate the mechanisms responsible for overpressured fluid states (Sleep & Blanpied 1992; Lockner & Byerlee 1994; Blanpied *et al.* 1998), and high-

light the essential role of fluid phases associated with healing and restrengthening (Nakatani & Scholz 2004; Tenthorey & Cox 2006). Byerlee (1990) and Rice (1992) suggest an upward migration of fluids within the damaged fault zone, treating the fault as a sealed conduit, thus explaining the apparent weakness of large faults. Depending on local material properties and rupture histories, fluid pathways can have complex structures (Miller 2006; Sibson 2007), thus leading to heterogeneous and asymmetric patterns of fluid driven processes. The spatially and temporally highly variable distribution of different volatile phases across a fault network, and its multitudinous geochemical, hydrothermal and mechanical implications suggest that an equilibrated state is improbable.